SAE 2007-01-4063
SAND2007-5600C

Effect of Intake Pressure on Performance and Emissions in an Automotive Diesel Engine Operating in Low Temperature Combustion Regimes

Will F. Colban and Paul C. Miles
Combustion Research Facility, Sandia National Laboratories, Livermore, CA, USA

Seungmook Oh
Korea Institute of Machinery and Materials, Daejeon, S. Korea

ABSTRACT

A single-cylinder, light-duty, diesel engine was used to investigate the effect of changes in intake pressure (boost) on engine performance and emissions in low-temperature combustion (LTC) regimes. Two different LTC strategies were examined: a dilution-controlled regime characterized by high rates of exhaust gas recirculation (EGR) with early-injection (roughly 30° BTDC), and a late-injection (near TDC) regime employing moderate EGR levels. For both strategies, moderate (8 bar IMEP) and low (3 bar IMEP) load conditions were tested at intake pressures of 1.0, 1.5, and 2.0 bar.

For both LTC strategies, increased intake pressure reduces emissions of unburned hydrocarbons (UHC) and CO, with corresponding improvements in combustion efficiency and indicated specific fuel consumption (ISFC), particularly at high load. Depending on the operating condition, UHC and CO emissions can stem from either over-lean or over-rich mixtures. UHC emissions can be further impacted by fuel from quench layers and liquid films. Increased intake pressure also reduces peak soot emissions at high load and shifts the peak soot emissions (the soot "bump") towards lower oxygen concentrations. Due to this shift, the influence of intake pressure on soot emissions differs for different oxygen concentrations. Soot emissions are reduced with increased intake pressure at high oxygen concentrations, but increased at low oxygen concentrations. Already low NO_x levels are reduced further at high intake pressures, though the influence of intake pressure is small compared to the influence of oxygen concentration.

Comparisons of the two LTC strategies at a fixed NO_x emission index of 0.5 g/kg-fuel show that late-injection LTC offers improvements in engine noise and soot over dilution-controlled LTC. Conversely, dilution-controlled LTC yields lower emissions of UHC and CO and better combustion efficiency and ISFC than late-injection LTC.

INTRODUCTION

Light-duty vehicles worldwide must now meet strict emissions standards, which dictate very low emissions of NO_x, particulate matter (soot), CO, and unburned hydrocarbons (UHC). Conventional diesel combustion systems suffer from high NO_x and soot emissions, while producing low levels of CO and UHC. To reduce NO_x and soot emissions, low-temperature combustion (LTC) strategies are being developed. One method of achieving LTC is to employ significantly reduced charge oxygen concentrations, which lowers engine power density. Mixing fuel and O_2 also becomes more difficult, and lower combustion temperatures slow CO and UHC oxidation rates. Both of these factors can lead to high CO and UHC emissions—especially at higher loads.

Turbochargers are used extensively in both large and small diesel engines to increase maximum power while reducing fuel consumption. With the development of variable-geometry turbochargers, turbochargers have become more versatile, allowing optimization over a larger operating range. Although the benefit of boosting the intake pressure on increasing the diesel's power density is clear, a better understanding is needed of the effects of intake pressure on emissions, combustion noise, and efficiency.

When studying the effects of intake pressure, it is important to first understand how a change in boost pressure affects the in-cylinder conditions during the fuel injection and combustion processes. Higher boost pressure raises the ambient in-cylinder density (ρ_{amb}) during the injection and combustion processes. Ambient density plays an important role in fuel jet vaporization, mixing, and penetration. Naber and Siebers [1] found

that diesel jets under higher ambient density conditions have shorter penetration distances and greater dispersion angles, resulting from a higher air entrainment rate into the spray. Higher entrainment rates are also evidenced by reductions in liquid length (Siebers [2]). In the long-time limit or far-field of a diesel jet, the analysis of Naber and Siebers [1] indicates that the rate of air entrainment scales with $\rho_{amb}^{0.25}$. Thus, at a position within the fuel jet corresponding to a fixed time after the start of injection, an increase in ρ_{amb} will result in a lower average fuel-air equivalence ratio ϕ, but not dramatically so. Increasing ρ_{amb} by a factor of 2 will decrease ϕ by less than 20%.

Although the entrainment rate increases with increasing ambient density, both lift-off length (Siebers and Higgins [3]) and ignition delay (Pickett et al. [4]) are decreased, resulting in less available time for entrainment and mixing prior to combustion. Pickett and Idicheria [5] have shown that the net result is an increase in ϕ at the time of ignition, or at the lift-off length for quasi-steady jets. Increased ϕ increases soot production—an expectation consistent with significantly increased observed soot formation with increasing ambient density over a broad range of ambient oxygen concentrations. The magnitude of the increased soot formation, however, is considerably larger than can be accounted for by the increase in ϕ. Moreover, for a given change in ambient density, the relative increase in soot formed is larger at lower oxygen concentrations. Pickett and Idicheria [5] also noted a competing effect: increased ambient density tends to improve air-fuel mixing throughout the combustion process, which results in higher soot oxidation rates.

Engine-out soot levels are a result of competition between formation and oxidation processes. There have been relatively few studies comparing engine-out emissions at various boost levels, and these studies have been restricted to heavy-duty diesel engines [6, 7]. Tanin et al. [6] reported that soot emissions generally decrease with increased intake pressure (at fixed load and NO_x), although at the highest boost soot increased under some operating conditions.

The measurements of Noehre et al. [7] clarify how intake pressure can affect soot emissions differently depending on the operating condition. Their data show that, as intake pressure increases, the EGR rate at which peak engine-out soot occurs is shifted toward higher values. However, neither the magnitude nor the width of the peak (the soot "bump") changes significantly. When the soot emissions are re-plotted against oxygen concentration this trend remains, although it is not as pronounced—as seen in Figure 1. Nevertheless, it is clear that at low $[O_2]$, increased boost will increase soot emissions, while at higher $[O_2]$ soot emissions will be reduced. At intermediate $[O_2]$ the soot will first be increased as boost pressure increases, subsequently decreasing as boost is further increased.

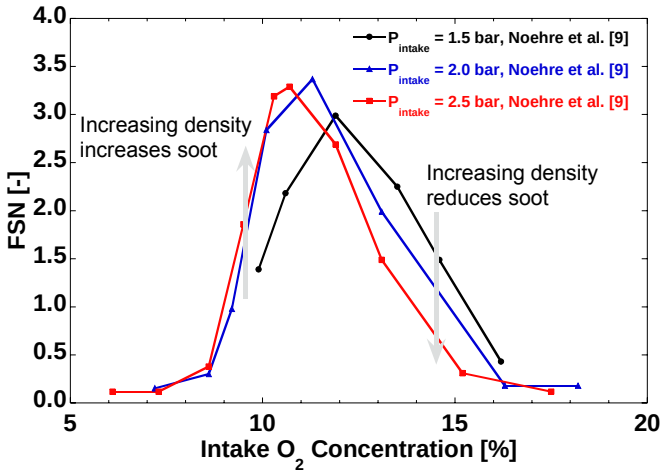

Figure 1. Soot filter smoke number levels at 8 bar IMEP versus $[O_2]$ from the heavy-duty diesel study of Noehre et al. [9].

Keeping in mind the result of Pickett and Idicheria [5]—that soot formation increases with ambient density for all $[O_2]$—the engine-out soot trends observed by Noehre et al. [7] imply:

- At high $[O_2]$, the benefits of increased mixing rates with increased boost during the soot oxidation phase outweigh the disadvantage of the relatively small increased formation rates.

- At low $[O_2]$, the higher mixing rates cannot overcome the combined disadvantages of lower oxidant in the ambient and the greater relative formation.

- At intermediate $[O_2]$, increased formation initially dominates, but with further increases in boost pressure increased mixing rates are able to compensate and soot emissions decrease.

An extension of this reasoning suggests that for automotive size diesels, which can maintain higher mixing rates in the expansion stroke due to flow motion, the influence of increased oxidation rates may be more pronounced and push the transitional (intermediate) $[O_2]$ to lower values. Currently however, there are no data available from which this conjecture can be tested.

From the above discussion, it is apparent that a great deal is known or can be surmised about the influence of ambient density (boost) on soot. Far less is known regarding the influence of ambient density on the remaining regulated emissions. In the work of Tanin et al. [6], it was found necessary to first retard, then advance, SOI as boost was increased to maintain constant NO_x. Noehre et al. [7] also measured NO_x, UHC, and CO emissions for intake pressures ranging from 1.5 bar to 2.5 bar at a moderate load condition of 8 bar IMEP. For a fixed EGR rate, they reported an increase in NO_x emissions with increasing boost, while UHC and CO emissions decreased. When the data are replotted against $[O_2]$, however, the trends are far less clear.

In light duty engines, CO emissions under some LTC operating conditions are thought to be heavily influenced by under-mixed fuel (Kook et al. [8] and Opat et al. [9]). Facilitating fuel-charge mixing by increasing boost thus seems one possible method to alleviate high CO emissions. Likewise, factors such as fuel spray over-penetration and liquid film formation—which influence HC emissions—are of greater concern in light-duty engines. A careful evaluation of the influence of boost on these factors has not yet been made.

This paper provides a systematic study characterizing engine-out emissions and combustion characteristics at intake pressures ranging from 1.0 to 2.0 bar for a single-cylinder, light-duty, automotive diesel engine. UHC, CO, NO_x, and soot emissions were measured for two separate LTC regimes—one characterized by high dilution and early injection ("dilution-controlled" or "PPCI-like") and the other by more moderate dilution but late injection ("MK-like"). Both low and moderate load conditions were investigated.

EXPERIMENT

The following sections provide a brief description of the research engine and emissions instrumentation, as well as an outline of the operating conditions and test matrix for this study. Additional details can be found in a previous study by Colban et al. [10].

RESEARCH ENGINE

The optically-accessible single-cylinder research engine was modified from a General Motors 4-cylinder 1.9 liter production engine. The head was outfitted with 4 valves angled 2° from vertical and a central, vertical Bosch CRIP 2.2 injector, supplied from a common rail. A Kistler 6125B quartz pressure transducer has been mounted in the production glow plug position. Plenum chambers with 80 times the engine displacement volume provide a constant pressure boundary at the intake runner inlet and exhaust runner exit. The main specifications of the engine and fuel injection system are listed in Table 1.

Figure 2 shows a dimensionally accurate cross-section of the research engine, including the bowl geometry. Although this engine design is intended for optical measurements, the results presented here did not require the use of optical techniques. Therefore, a metal piston was used for the experiments and the optical window ring forming the upper cylinder liner was fitted with metal window inserts (illustrated in Figure 2). Despite the use of metal components for this study, the optically-accessible nature of the engine design leads to certain features that distinguish it from conventional all-metal test engines. The most substantial difference is the increased size of the top ring-land crevice, which reduces the geometric compression ratio from a metal-engine target of 17.4 to 16.7 for the optical design. The other notable design feature resulting from optical accessibility is that the windows surrounding the upper portion of the cylinder limit cooling of the cylinder wall in that region. Limited wall (and piston) cooling contributes to the need to skip-fire the engine in order to avoid overheating.

Table 1. Engine and Fuel Injector Specifications

Engine Specifications	
Bore:	82.0 [mm]
Stroke:	90.4 [mm]
Displacement Volume:	477 [cm^3]
Geometric CR:	16.7
Squish Height:	0.78 [mm]
Swirl Ratio:	2.2
Engine Speed:	1500 RPM

Valve Events (0.15 mm lift)			
IVO:	-359°CA	EVO:	132°CA
IVC:	-152°CA	EVC:	360°CA

Fuel Injector	
Number of Holes:	7
Included Angle:	149°
Sac Volume:	0.12 [mm^3]
Nozzle Hole Diameter:	0.14 [mm]
Rail Pressure:	860 bar
Bosch Flow Number:	440 [cc/30 sec]
Fuel:	#2 Diesel

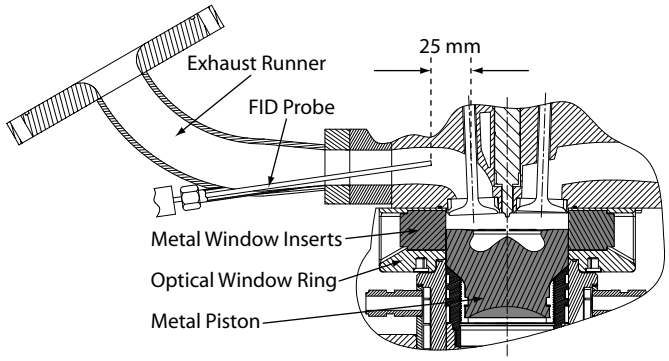

Figure 2. Schematic of the engine showing the location of the fast-FID probe. The piston bowl geometry shown is a faithful representation of the production-engine bowl shape.

EMISSIONS EQUIPMENT

A Cambustion HFR 400 fast flame ionization detector (FID), equipped with a heated sampling line and a constant pressure system, was used to measure wet UHC in the exhaust port. The probe tip was located approximately 25 mm from the exhaust valve stem, as shown in Figure 2. The fast-FID response time is roughly 0.5 ms (4.5°CA at 1500 RPM), allowing time-resolved UHC measurements from the exhaust stream. The probe transit time—the time required for the sample to travel from the probe tip to the FID—was about 3.5 ms (31.5°CA at 1500 RPM). A dynamic, in-situ calibration was performed using a span gas containing propane at 950 ppm. During the calibration procedure, the engine was skip-fired to remove the influence of temperature and pressure variations.

Soot was measured using an AVL 415S smoke meter, with the sample taken from the exhaust gases downstream of the exhaust plenum. No correction was made to the measured smoke numbers to compensate for skip-fired operation. NO_x emissions were measured using a California Instruments 600 Heated Chemiluminescent NO/NO_x Analyzer (HCLD). The range was toggled between 0-30 ppm and 0-300 ppm, depending on the NO_x levels at each operating condition. Exhaust levels of CO and CO_2 were measured with a California Instruments 300 Nondispersive Infrared (NDIR) Gas Analyzer. The range of measurable CO levels was 0-6000 ppm, while CO_2 had a range of 0-15%. A condenser removed water and condensable hydrocarbons from the sample before analysis by the HCLD and NDIR.

OPERATING CONDITIONS

All of the tests reported here were performed at an engine speed of 1500 RPM and a constant injection pressure of 860 bar. The test matrix for this study is summarized in Table 2, which describes the engine loads, intake oxygen concentrations, and injection timings that were investigated at each intake pressure.

Simulated EGR was used to obtain the desired O_2 concentrations by combining air, N_2, and CO_2 in the inlet stream. The relative proportions were determined by matching the specific heat (C_p) of the simulated EGR to that of engine exhaust gases (assuming complete combustion of the fuel) at 600 K. At a fixed boost level the proportions of air, N_2, and CO_2 were varied to obtain different O_2 concentrations. However, the total inlet mass flow rate was held constant at each boost level to maintain a constant TDC density. Because changes in intake charge composition affect the specific heat ratio (C_p/C_v) of the mixture, the intake temperature was varied to maintain a fixed adiabatic core temperature at TDC of 935 ± 7 K. Intake temperatures ranged from roughly 100°C for 8% [O_2] to 80°C for 17% [O_2]. For a given O_2 concentration, increases in boost were achieved by holding the relative proportions of air, N_2, and CO_2 fixed, while increasing the overall inlet mass flow rate.

The dilution-controlled LTC regime features high rates of EGR and low [O_2], which lowers combustion temperatures and provides an increased ignition delay to assist with pre-combustion mixing. It is similar to Toyota's "smokeless-rich" combustion [11] or AVL's "dilution-controlled" combustion system (DCCS) [12]. For the dilution-controlled LTC regime, the molar O_2 concentration ([O_2]) was varied from 8% to 17% at three values of intake pressure: a naturally-aspirated condition of 1.0 bar and two boosted conditions of 1.5 and 2.0 bar. At 1.0 bar intake pressure, combustion did not occur below 11% [O_2] at either load condition. The fueling rate was held constant for any given [O_2] sweep, as described below. Maximum brake torque (MBT) injection timing was used at each [O_2] condition. Figure 3 shows the start of injection (SOI) at MBT timing for the [O_2] sweeps. Earlier SOI is required to maintain the same nominal load as [O_2] decreases. In this paper, SOI is designated as either the start of injection command (SOI_c), meaning the energizing of the solenoid, or the actual start of injection (SOI_a). Estimates of SOI_a are used only for calculations of ignition delay and to illustrate the spray targeting on the piston.

The late-injection LTC regime is similar to the modulated kinetics concept introduced by Nissan [13], the main difference being that the current study features only a moderate swirl ratio of R_s = 2.2. The late-injection LTC regime was investigated by performing SOI sweeps at intake pressures of 1.5 and 2.0 bar. A fixed O_2 concentration of 15%, representing a moderate EGR rate, was chosen. To illustrate the emissions behavior as injection timing is retarded towards TDC, results are shown from SOI_c = -25°CA down to 0°CA. The fueling rate was held constant at each load condition during these SOI sweeps.

For both LTC regimes, the effect of load was explored by testing two loads at each boost level: a low load of nominally 3 bar gross IMEP and a moderate load of nominally 8 bar IMEP (the maximum achievable load at 1.0 bar boost was approximately 6 bar IMEP at 11% [O_2]).

Fueling rates for each boost level were determined by

Table 2. Test Matrix

Dilution-Controlled LTC

Boost [bar]	IMEP [bar]	O_2 Conc. [%]	SOI_c [°CA]
1.0	3 & 6	11 – 17	MBT (Fig. 3)
1.5	3 & 8	8 – 17	MBT (Fig. 3)
2.0	3 & 8	8 – 17	MBT (Fig. 3)

Late-Injection LTC

Boost [bar]	IMEP [bar]	O_2 Conc. [%]	SOI_c [°CA]
1.5	3 & 8	15	-25 to 0
2.0	3 & 8	15	-25 to 0

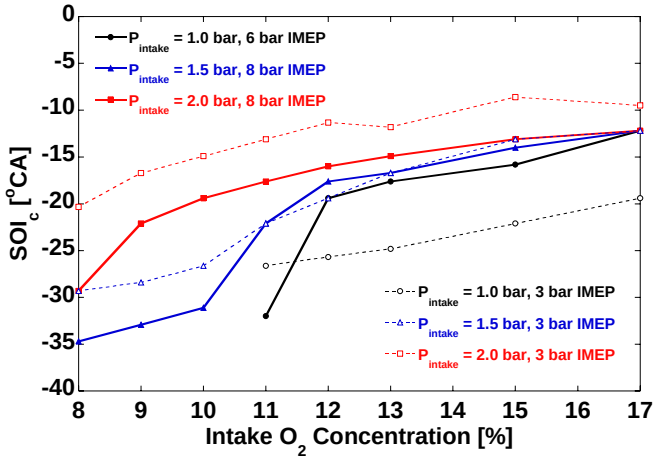

Figure 3. MBT timing given as SOI_c for the O_2 concentration sweeps.

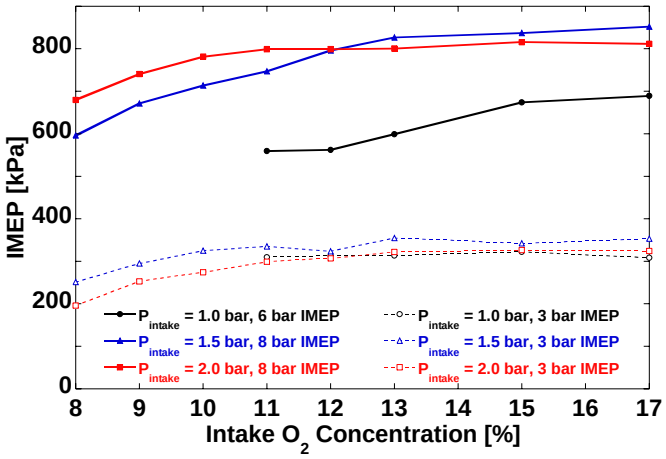

Figure 4. IMEP variation at MBT timing for the O_2 concentration sweeps.

varying the injection duration to closely match IMEP at 12% [O_2] to either 3 bar (low load condition) or 8 bar (moderate load condition). Boost was found to have a very weak effect on the injection duration. Accordingly, injection durations (and hence fueling rates) were a function primarily of load, were independent of [O_2] and SOI, and varied slightly with boost. Despite the use of fixed fueling at each load/boost condition, the IMEP achieved differed somewhat from the nominal values reported in Table 2. Figure 4 illustrates the IMEP variation for the [O_2] sweeps, and shows that IMEP falls-off at lower [O_2]. This decline in IMEP was accompanied by a corresponding drop in combustion efficiency (discussed later and shown in Figure 21). IMEP variation was less significant for the SOI sweeps with overall IMEP remaining fairly constant (Figure 5), although a slight decline in IMEP was observed at both early and late injection timings. Despite a drop-off in IMEP at low [O_2] and late-injection, no misfires were observed. Furthermore, IMEP COV levels were primarily dependent on load, with roughly constant levels of 1% at 8 bar and 2% at 3 bar. At low load, COV levels increased to approximately 3.5% as intake [O_2] was decreased to 8%.

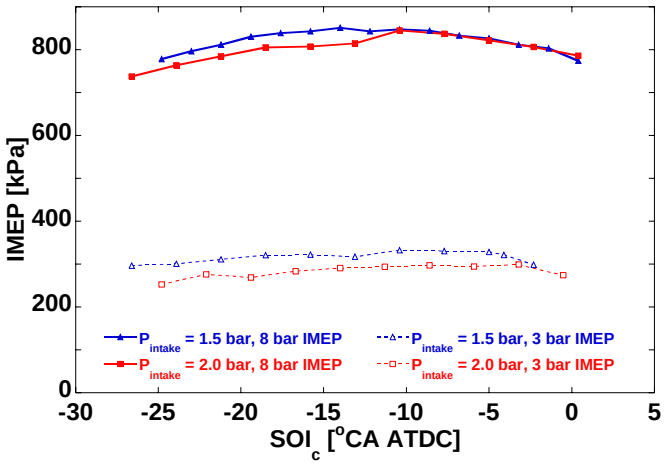

Figure 5. IMEP variation for the SOI sweeps, plotted as SOI_c.

Table 3. Operating Conditions

Dilution Controlled LTC

Boost [bar]	P_{ex} [bar]	EGR [%]
1.0	1.53 ± 0.02	Fig. 6
1.5	1.73 ± 0.02	Fig. 6
2.0	2.13 ± 0.03	Fig. 6

Late-Injection LTC

Boost [bar]	P_{ex} [bar]	EGR [%]	
		3 bar IMEP	8 bar IMEP
1.5	1.87 ± 0.07	62.7	39.5
2.0	2.29 ± 0.04	73.2	47.8

The engine was operated in a skip-fired mode, with fuel injection occurring once every four cycles. Even with skip-firing, the engine run times were limited, and it was not possible to achieve a true steady state of operation. Because of the transient nature of the engine operation, a rigid testing schedule was followed to ensure that measurements were made at the same thermal state for each test. Prior to commencing skip-firing, the engine was motored for 2 minutes, allowing the intake pressures to stabilize and the combustion chamber surfaces to preheat. The engine was then skip-fired for 1 minute, permitting the gas composition in the exhaust plenum to stabilize and allowing the outputs from the emissions analyzers to reach an approximately steady value. Following this period, sampling of cylinder pressure, gaseous emissions, and soot began simultaneously. Because the gas composition in the exhaust plenum still changes slightly during the sampling period, we adhered strictly to the time schedule described above to ensure that these changes affected the measured emissions equally for each data set. Pressure and gaseous emissions were sampled at 0.25°CA resolution for 75 skip-fired cycles (representing 300 total engine cycles). After taking a data set, the engine was stopped and allowed to cool for 6 minutes before repeating the test procedure for the next data set.

The intake plenum pressure varied by less than ±0.05 bar for each reported boost condition. The exhaust plenum pressure was dependent on the intake conditions, with values given in Table 3, including the range for each value. Also shown in Table 3 are the equivalent EGR rates for the late-injection LTC regime cases. Equivalent EGR rates are computed for each load, boost, and [O_2] assuming complete combustion of the fuel. Equivalent EGR rates for the cases in the dilution-controlled LTC investigation are shown in Figure 6 plotted against [O_2]. The EGR rate is defined as the ratio of recirculated exhaust mass to total intake mass.

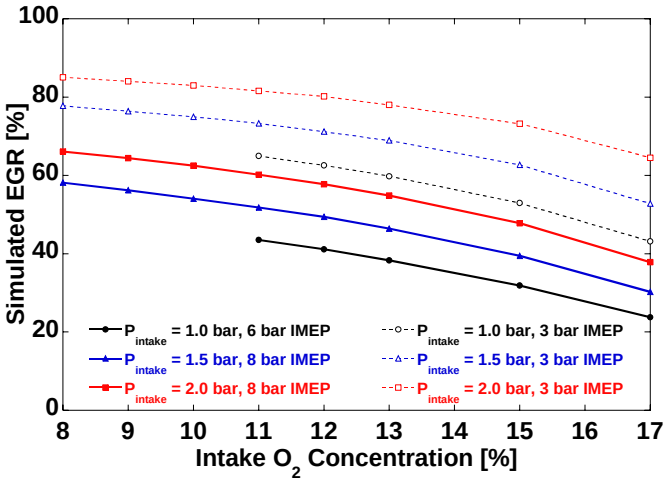

Figure 6. EGR rates for the O_2 concentration sweeps.

Despite the differences in engine geometry and cooling, and the use of both skip-firing and simulated EGR, we have observed very good agreement in measured engine-out emissions and combustion performance metrics when compared against results obtained in an all-metal test-engine with the same combustion system design and at the same operating conditions. A detailed description of this comparison will be forthcoming in a separate publication.

DATA ANALYSIS

PRESSURE

The pressure data were averaged over 75 fired cycles, and used to calculate indicated mean effective pressure (IMEP), apparent heat release rate (AHRR), and the ignition delay periods. Motored pressure data were also taken at each operating condition, and used in the heat release analysis to partially compensate for crevice flows and heat losses. The heat release analysis was performed following an iterative two-zone procedure using temperature and mixture dependent gas properties, as described by Kook et al. [14].

Combustion burn angles were computed from the integrated apparent heat release, and used to determine ignition delay, ignition dwell, and burn durations. Ignition delay was computed as the difference between the start of combustion, as estimated using the 10% burn angle (BA10), and SOI_a. The lag between SOI_c and SOI_a was approximately 400 μs (3.65°CA) for all conditions. Ignition dwell times were calculated as the difference between end of injection (EOI) and BA10. EOI was determined from injection rate measurements performed at the University of Wisconsin (Opat, et al. [15]). Injection durations lasted approximately 6.15°CA for low load conditions and 10.10°CA for moderate load conditions.

EMISSIONS

To determine the emissions index for each species from the gaseous emissions data, it is first necessary to convert the cycle-resolved UHC data to a cycle-averaged UHC concentration. The fast-FID data conversion procedure obtains cycle-averaged emissions by integrating the cycle-resolved UHC mass emissions over the exhaust period, using one-dimensional modeling to estimate the instantaneous exhaust gas mass flow. Following this conversion, wet mole fractions of the remaining exhaust species are computed and used to calculate the emissions index reported here. Details of the UHC conversion procedure and emissions analysis are provided by Colban et al. [10].

SIMULATIONS

To aid in the interpretation of the data, constant volume, closed homogeneous reactor simulations using Chemkin 4.1 [16] were performed. In these simulations, the initial equivalence ratio and mixture temperature were specified, as well as an initial pressure of 40, 60, or 80 bar. These pressures correspond closely to the pressures at the start of combustion observed in the O_2 concentration sweeps for the three boost levels investigated. A detailed kinetic mechanism for *n*-heptane [17] supplemented with nitrogen chemistry [18] was used. The initial mixture temperature was specified to be the mixture temperature achieved when a quantity of fuel corresponding to the desired equivalence ratio is heated from an initial temperature of 360 K, vaporized, and mixed adiabatically with the ambient gases at 935 K. An ambient gas O_2 mole fraction of 0.12 was specified for all runs, corresponding to a mixture of real air with the required quantity of the products of complete, stoichiometric *n*-heptane combustion.

It must be borne in mind that these simulations correspond to a great simplification of the actual processes occurring in an engine, and represent results that would be obtained if the injected fuel mixed rapidly to the specified equivalence ratio, and then reacted with no further mixing. Despite this simplification, we believe they provide a useful indication of the time scales of the chemical processes occurring at the relevant temperatures and pressures, as well as an indication of the effects of pressure on both the rates and equilibria of the chemical reactions occurring.

RESULTS AND DISCUSSION

We begin with a discussion of the effect of increased boost on the in-cylinder conditions near the start of injection and during combustion. The emissions and combustion performance results follow, divided into two sections to discuss the dilution-controlled and late-injection LTC regimes separately. Finally, a performance-based comparison will be made between the two LTC regimes, highlighting the advantages and disadvantages of both.

IN-CYLINDER CONDITIONS

Increasing boost pressure has a number of effects on in-cylinder conditions. When O_2 concentration is held constant as boost pressure is increased, the total in-cylinder O_2 mass increases. Because the fueling rate is approximately constant, the higher O_2 mass drives down the global fuel-air ratio, creating an overall leaner mixture. Global equivalence ratios for each test are shown in Figure 7, illustrating the drop in average equivalence ratio with increasing boost pressure. The leaner mixture results in a higher O_2 concentration in the exhaust, and a higher EGR rate is thus required to maintain a fixed O_2 concentration, as was shown in Figure 6.

Figures 8 and 9 show the ambient in-cylinder density at SOI_c for the $[O_2]$ and SOI sweeps, respectively. Density was calculated from the known intake mass flow rate, an estimate of the residual trapped mass inside the cylinder at TDC intake (this engine has very little overlap—see Table 1), and the cylinder volume at each crank angle. The significant differences in ambient density between the low and moderate load conditions at each boost condition for the $[O_2]$ sweeps are primarily due to differences in SOI at MBT timing (see Figure 3). Smaller differences observed as load is varied for the SOI sweeps are due to higher residual gas temperatures at the higher load (residual gas temperatures were estimated using a 1-D combustion simulation model in WAVE v7.1).

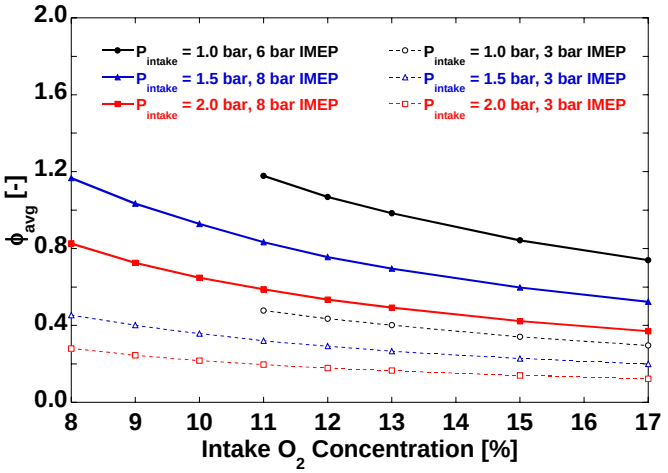

Figure 7. Average equivalence ratio for the O_2 concentration sweeps.

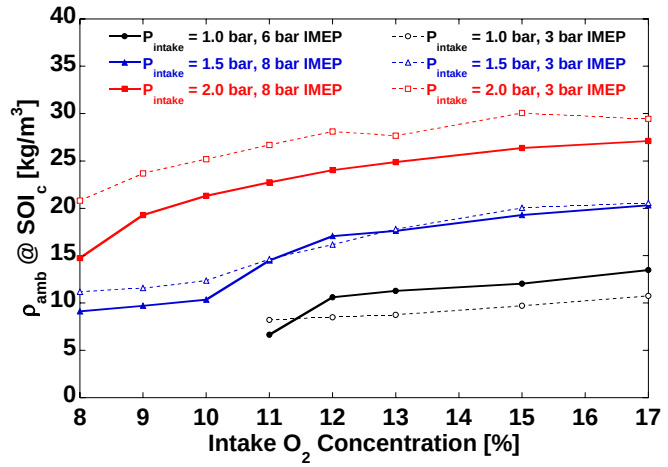

Figure 8. Ambient in-cylinder density at SOI_c for the O_2 sweeps.

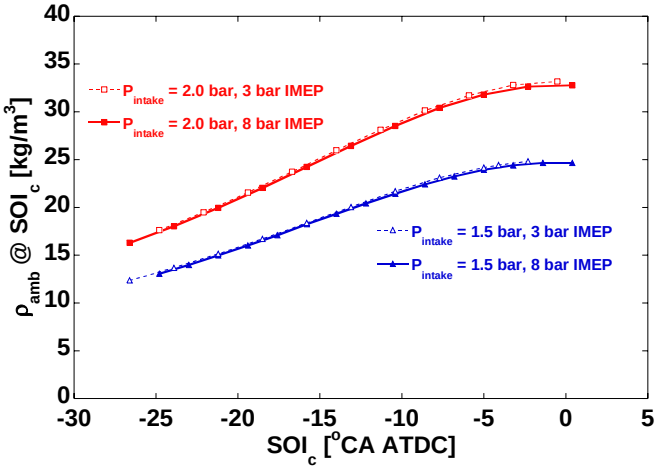

Figure 9. Ambient in-cylinder density at SOI_c for the SOI sweeps.

DILUTION-CONTROLLED LTC COMBUSTION

Cylinder Pressure Analysis

The maximum pressure rise rate (MPRR) was computed as a surrogate for a direct measurement of combustion noise, and is shown in Figure 10. At the higher load, where engine noise is greater, increases in boost show significant reductions in MPRR, across the entire range of $[O_2]$ tested.

Reduced MPRR with increased boost pressure can be largely attributed to a significant reduction in ignition delay with increased ambient density for both load conditions (Figure 11). Although $[O_2]$ is held constant as boost is increased, reduced ignition delay is caused by greater absolute O_2 number density at higher boost. Arrhenius type correlations for ignition delay typically incorporate an inverse dependence on ambient pressure [19] to account for the increased density, behavior which

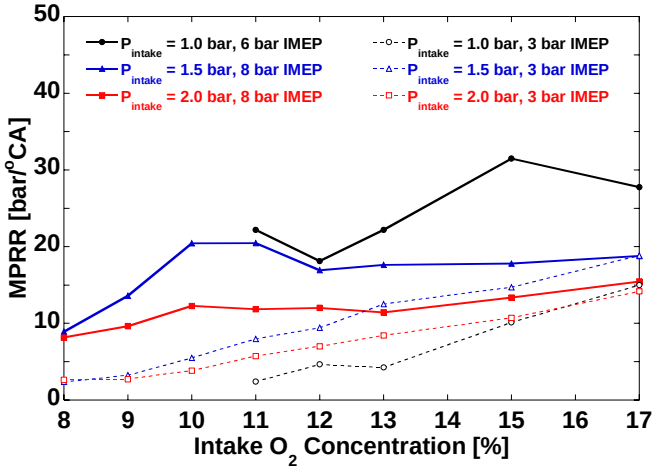

Figure 10. Maximum cylinder pressure rise for the $[O_2]$ sweeps.

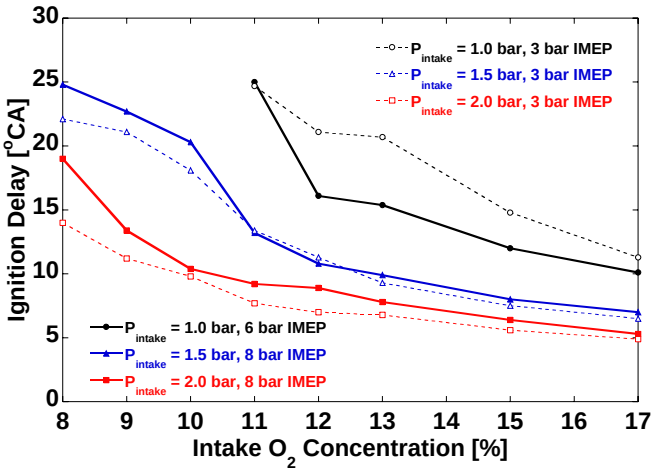

Figure 11. Ignition delay for the [O_2] sweeps. Ignition delay is defined as the time from the actual start of injection (SOI_a) until the 10% burn angle.

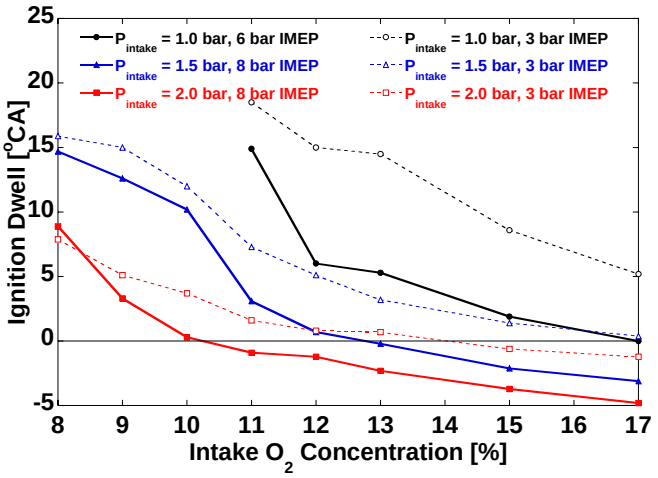

Figure 12. Ignition dwell for the O_2 concentration sweeps, where ignition dwell is defined as the time from the end of injection (EOI) until the 10% burn angle.

is approximated by the ignition delay results of Figure 11. The reduction in premixing time associated with decreased ignition delay must be juxtaposed with the expected increase in mixing rates associated with increased ambient density (boost). Anticipating that the $\rho_{amb}^{0.25}$ scaling of mixing rate observed in free jets holds during the initial mixing period in our engine, we expect that the stronger pressure/density dependency of ignition delay will dominate. Thus, for representative mixing rate scaling, increases in boost will likely result in less premixing at the time of ignition—as has been observed in free jets by Pickett and Idicheria [5].

Another important parameter that has been shown to have an effect on emissions in heavy-duty diesel engines [20] is ignition dwell, defined as the time between end of injection (EOI) and start of combustion. Generally, UHC emissions increase rapidly when ignition dwell becomes positive, which indicates that ignition occurs after the end of injection. Figure 12 shows the calculated ignition dwell times as [O_2] is varied, where start of combustion was approximated using the 10% burn angle. As both boost and [O_2] increases, ignition dwell drops, indicating that in some cases, especially at high boost, a significant portion of the fuel is injected after combustion has already begun.

Finally, to illustrate the influence of ambient density on mixing rates late in the combustion event, BA70-90 burn durations are shown in Figure 13. By BA70, experience suggests that—for the relatively advanced MBT injection timings employed—the remaining heat release will be dominated by diffusion- or mixing-controlled combustion. Hence, a comparison of BA70-BA90 durations for various boost levels will provide an approximate measure of the relative mixing rates. With the exception of the light load, naturally-aspirated operating condition, BA70–BA90 is found to decrease as boost level is increased. Focusing on the results obtained at 1.5 and 2.0 bar intake pressures, we see that in this late-mixing period increased ambient density increases mixing rates uniformly. That is, there is roughly a 33% decrease in

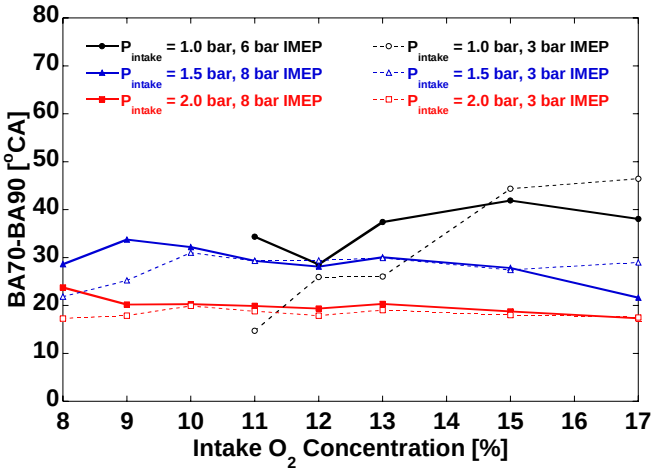

Figure 13. 70-90 burn angle times for the [O_2] sweeps, indicating the relative duration of the later mixing-controlled combustion.

BA70-BA90 across the entire range of [O_2] as boost increases from 1.5 to 2.0 bar.

UHC Emissions

The effect of boost pressure on the UHC emissions index at two different load conditions is shown in Figure 14. There is an overall trend of increased UHC at lower O_2 concentrations, which is characteristic of this dilution-controlled LTC regime [11, 12]. Generally, emissions of UHC are lower at the higher load, the exception being when the global equivalence ratio approaches or exceeds 1 (Figure 7). At these conditions, dramatic increases in UHC are observed, particularly at the higher loads and lower intake pressures. The trend of rapidly increasing UHC at near-stoichiometric conditions was also noted in the heavy-duty diesel study by Noehre et al. [7]. Increased boost pressure reduces UHC, and is especially effective at high load and lower [O_2] where UHC emissions are highest.

UHC emissions correlate closely with the ignition dwell times shown in Figure 12. Over-lean regions formed during the ignition delay period are known to be a

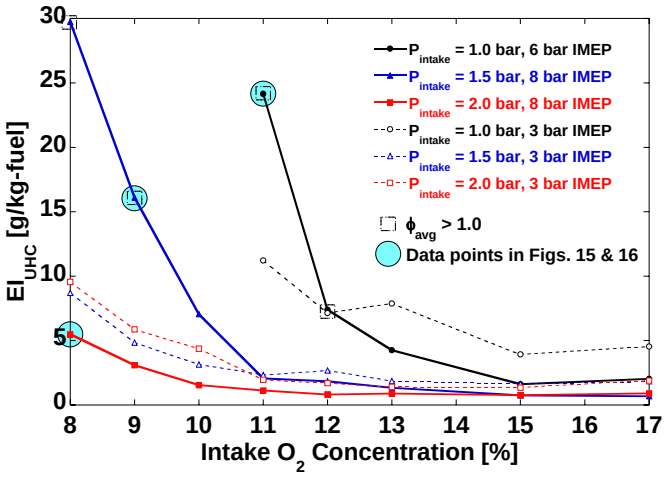

Figure 14. UHC emissions indices for the [O_2] sweeps. The data points enclosed in boxes correspond to data obtained with global equivalence ratios greater than 1.0, and the filled circles designate data points which are examined more closely in Figures 15 and 16

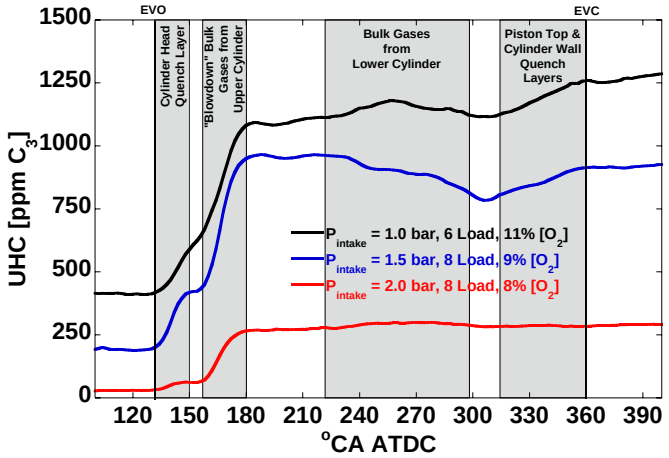

Figure 15. FID traces of cycle-resolved UHC emissions in the exhaust port. EVO and EVC times are indicated, as well as periods corresponding to specific sources of UHC.

dominant source of UHC emissions in conventional diesel combustion systems [21]. Musculus et al. [20] argue that—for light-load, low-temperature combustion systems characterized by positive ignition dwell—over-lean mixtures are formed from the last fuel injected, which mixes rapidly with the ambient fluid. In light of the significant reduction in dwell time observed as ambient density is increased, this mechanism is consistent with the behavior observed here. However, for conditions where the global equivalence ratio approaches (or exceeds) 1, the lean "over-mixed" regions would need to substantially fail to mix with the remainder of the charge if UHC emissions stemming from these regions are to be significant. Under these conditions, other potential sources of UHC must also be considered, including: wall quench layers, partially-oxidized fuel fragments stemming from overly-rich ("under-mixed") regions, and delayed vaporization/mixing of fuel due to liquid film formation.

To assess the likely significance of each of these sources we shall examine the cycle-resolved UHC emission behavior provided by the fast-FID as well as estimates of spray penetration, liquid length, and UHC yield predicted in homogeneous reactor simulations. We will focus primarily on three cases, each at a different boost pressure, all of which have high UHC levels. Contrasting these three cases provides information on how increases in boost pressure can affect the contributions from different UHC sources.

Figure 15 shows the fast-FID traces for the three conditions—all at moderate load, low [O_2], and advanced SOI. Each FID trace has been averaged over 75 skip-fired cycles, and has been shifted such that the initial response of the probe corresponds with exhaust valve opening (EVO). As discussed in previous work [10] and indicated in Figure 15, the time-resolved fast-FID signal can be separated into distinct periods, which provide information on potential sources of UHC:

- Just after EVO, gases containing UHC from surface quench layers near the head and valves exit first. For advanced SOI, wherein a greater portion of the fuel jet enters the squish region, these UHC quench layers are expected to be more pronounced.

- During the subsequent blowdown phase, bulk gases are expelled from the upper portion of the cylinder, followed by a brief period of flow reversal near BDC.

- As the exhaust stroke progresses the remaining bulk gases, which were positioned lower in the cylinder at EVO, are forced out.

- Finally, UHC present in cylinder wall or piston top quench layers are ejected just prior to EVC. Like the head/valve region layers, these latter quench layers are also anticipated to be more significant with advanced SOI.

To further examine the potential for fuel jet penetration into the squish volume, is helpful to consider estimates of fuel jet targeting, penetration, and dispersion angle, calculated from the formulations given by Naber and Siebers [1] and Siebers [22]. The left-hand sides of the images shown in Figure 16 illustrate the spray penetration, dispersion angle, and relative position of the piston and injector tip at 2°CA after the actual start of injection ($ASOI_a$). Where spray penetration profiles overlap the piston bowl, impingement on the piston is implied.

For intake pressures of 1.0 and 1.5 bar, the fuel jet targeting at 2°CA $ASOI_a$ shows that a portion of the fuel vapor will enter the squish volume, while at 2.0 bar intake pressure little or no fuel vapor is expected to enter the squish volume. Apart from spray targeting, the reduction in penetration distance with increasing boost, which is evident from Figure 16, should also contribute to reduced fuel penetration into the squish volume. The FID traces in Figure 15 are consistent with the penetration and targeting schematics in Figure 16. A sharp rise in the UHC signal at EVO for the 1.0 and 1.5

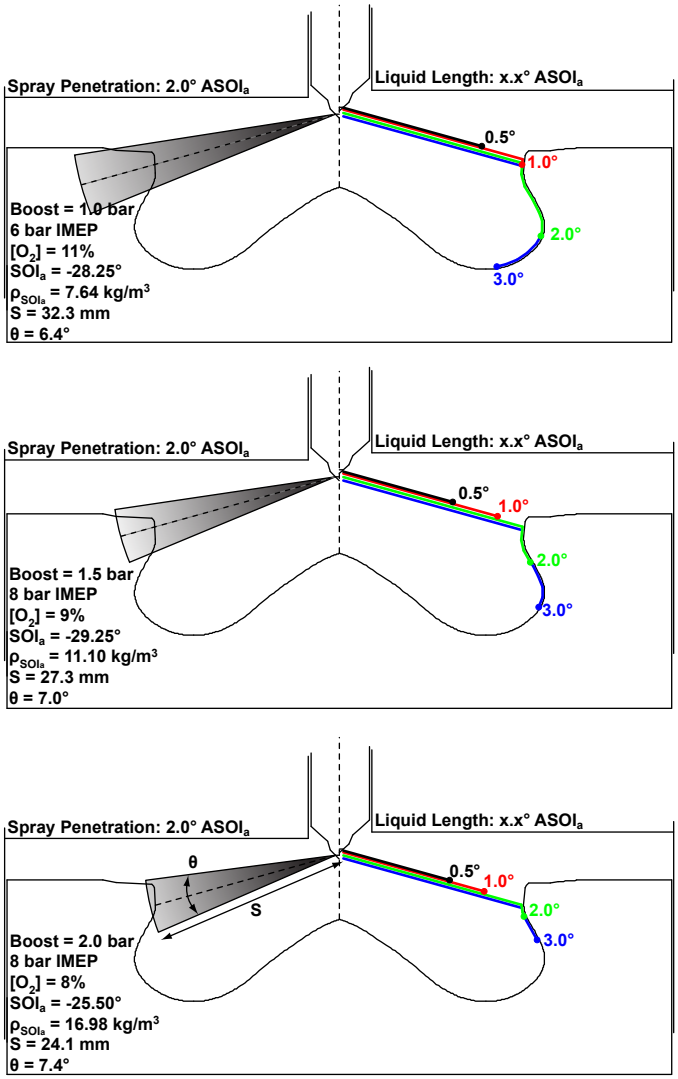

Figure 16. Schematics showing vapor penetration distances and dispersion angles on the left-hand column, and liquid length positions at certain times after the start of actual injection (ASOI$_a$) on the right-hand column.

bar cases, and a similar rise just prior to EVC, are indicative of significant UHC emission from fuel injected directly into the squish region. In contrast, very little increase near EVO, and no increase near EVC, is observed at 2.0 bar.

When the cycle-resolved UHC mass emissions are weighted by the instantaneous exhaust gas mass flow [10], it is found that the greater part of the UHC emissions are associated with the bulk gas exhaust periods. As noted above, bulk gas UHC emissions may stem from either overly-lean or overly-rich regions. Increasing boost increases mixing rates both during the fuel injection process, and during the latter portion of the combustion process (Figure 13), in addition to reducing the global equivalence ratio at a given O_2 concentration (Figure 7). It thus seems reasonable to assume that at least a portion of the decreased UHC emissions observed with higher intake pressures is due to improved mixing of overly-rich regions, especially for those operating conditions with global equivalence ratios approaching or exceeding 1. However, this increased mixing can only reduce UHC emissions stemming from regions with local equivalence ratios exceeding approximately 2, and thus may not be the dominant cause of the reduced UHC emissions.

In support of this statement, Figure 17 presents UHC concentrations predicted in constant volume homogeneous reactor simulations as a function of equivalence ratio, for three initial ambient pressures corresponding to the three boost conditions employed. Like previous observations that no soot is formed for diesel combustion at equivalence ratios less than approximately 2 [11, 23, 24], little UHC is found for $\phi < 2$—the majority of the fuel carbon is found in CO. UHC levels in Figure 17 are approximately 100 ppm at $\phi = 1.75$. A further observation to make from Figure 17 is that increased pressure (or ambient density) reduces the UHC mole fraction seen in the overly rich mixtures, though the difference is not large.

As discussed above in the context of the reduced maximum pressure rise rate observed with higher boost (Figure 10), increased intake pressures are likely to lead to richer mixtures at the time of ignition due to the shorter ignition delay. Consequently, UHC emissions stemming from overly lean regions are expected to be reduced by increased boost. Moreover, at a higher ambient density the rates of combustion of lean mixtures are increased significantly. Figure 18 presents the energy release rate of $\phi = 0.5$ mixture for three different initial ambient pressures. Note that halving the ambient density (pressure) results in a nearly 3-fold increase in the combustion duration—which still is not complete 4 ms after the start of the simulation for the lowest pressure condition.

Bulk gas UHC can also stem from a third source: delayed vaporization and mixing of the fuel until late in the cycle. For conventional diesel combustion in large-bore engines, UHC from this source is due to fuel emanating from the injector sac and hole volumes [21]. In light-duty engines, however, liquid films formed on the

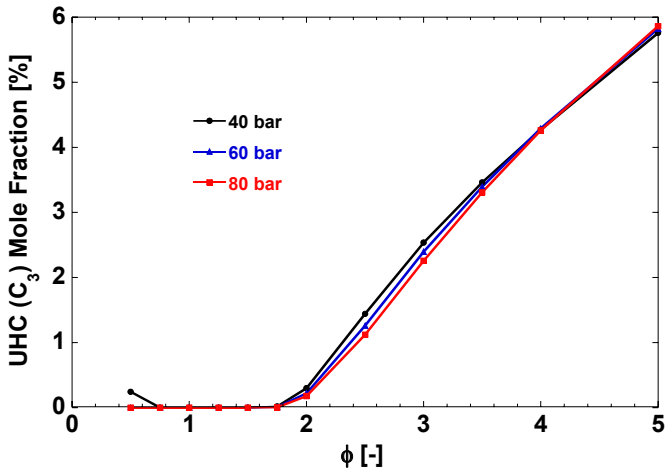

Figure 17. UHC mole fraction vs. equivalence ratio for three different initial ambient pressures, 4.0 ms (36°CA at 1500 rpm) after the actual start of reaction (ASOI$_a$).

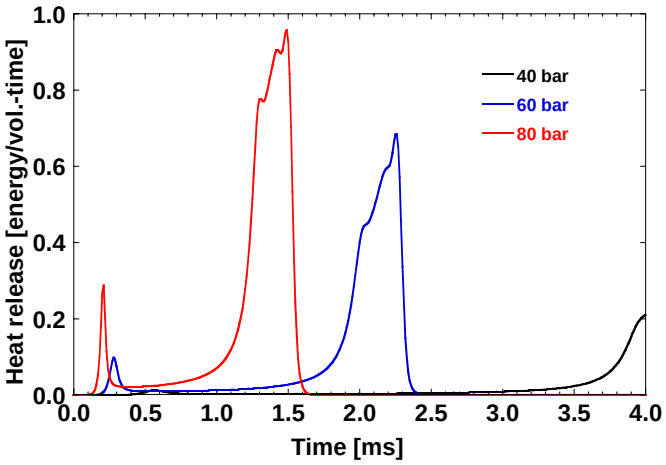

Figure 18. Heat release rates computed for three different initial ambient pressures (4.0 ms = 36°CA at 1500 rpm). ϕ = 0.5 for all three conditions.

piston can provide another mechanism for delayed vaporization and mixing.

To help assess the potential for liquid film formation on the piston surfaces, calculations of liquid length at each condition were made based on the correlation presented by Higgins et al. [25]. Figure 19 shows the predicted liquid lengths for each boost level and load at 5°CA $ASOI_a$, a time when the fuel jet would be fully developed in a quiescent chamber. Liquid impingement will occur when the distance along the spray from the injector nozzle to the piston surface is less than the liquid length. This distance changes with piston position. However, the minimum distance that can be attained is 22.5 mm—which is indicated on Figure 19. Conditions which have fully-developed liquid lengths less than the minimum impingement distance will not form liquid films. From these estimates we can conclude that the increased UHC observed at low $[O_2]$ for the 3 bar load, highest boost condition are unlikely to be associated with liquid film formation.

For liquid lengths longer than the minimum distance,

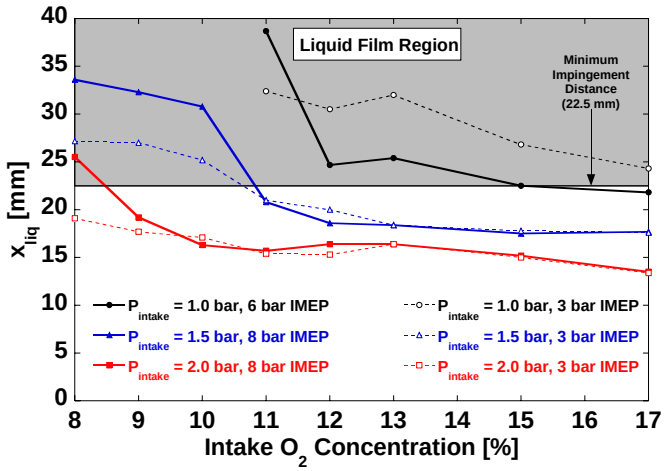

Figure 19. Estimated liquid lengths at 5.0° $ASOI_a$, with the darkened region indicating a distance which is greater than the minimum required for liquid impingement.

liquid impingement may or may not occur, depending on the injection timing. Film formation for these conditions must be evaluated on a case-by-case basis. Such an evaluation has been performed for the cases illustrated in Figure 16, and estimates of liquid length are shown on the right-hand sides of the schematics for a series of times $ASOI_a$. The injector and head surface positions are shown relative to the piston top at SOI_a. As the time sequence progresses, the position of the liquid portion of the fuel jet is denoted on the images for times 0.5°, 1.0°, 2.0°, and 3.0°CA $ASOI_a$. Times later than 3.0°CA $ASOI_a$ are not shown because they show little change in liquid length. For liquid lengths that are greater than the distance between the injector nozzle and the piston bowl, the resultant distance has been projected along the bowl surface. Furthermore, the change in position of the piston relative to the spray centerline has been accounted for as the injection event proceeds.

The anticipated reduction in liquid length with increased ambient density (boost) can be clearly seen in Figure 16. Nevertheless, for all three cases considered, liquid films could form on the piston surface, though they would likely be considerably larger at the lowest boost level. Kashdan et al. [26] have recently proposed that liquid films on the piston can undergo flash boiling during the expansion stroke, leading to UHC emissions. In this scenario, the films vaporize shortly after EVO when the cylinder pressure drops rapidly. As the piston descends further, vapor leaves the bowl and enters the bulk gases in the lower portion of the cylinder. This mechanism is consistent with the fast-FID traces of Figure 15 during the periods corresponding to bulk gas UHC emissions. At the lowest boost level, when liquid film formation is anticipated to be greatest, the FID traces indicate elevated UHC concentrations from lower in the cylinder.

Reinforcing the flash boiling hypothesis, imaging studies of combustion luminosity in gasoline direct-injection engines [27] show that flames associated with liquid film combustion lift off the piston top late in the cycle. However, piston-top liquid films are also observed throughout the expansion and exhaust strokes—perhaps composed of the heavier fuel components. Other studies have also noted persistence of liquid films for several engine cycles [28]. Returning to Figure 15, the initial UHC concentration prior to EVO is representative of the UHC remaining in the exhaust port after 3 motored cycles. A previous port-scavenging analysis [10] has shown that UHC from in-cylinder residuals and backflow into the cylinder during the motored cycles cannot account for the high remaining UHC levels. UHC storage in liquid films presents a possible mechanism for the poor apparent scavenging—UHC levels prior to EVO correlate well with the extent of liquid film formation indicated in Figure 16.

In summary, increased boost is expected to reduce UHC emissions stemming from both over-rich regions as well as over-lean regions. Boost can also reduce the formation of liquid films and their contribution to UHC

emissions. In-cylinder measurements of UHC distributions and speciated exhaust gas measurements would be helpful to clarify the relative contributions of each of these sources and how they change with boost.

CO Emissions

Trends in CO emissions, shown in Figure 20, are similar to those of UHC, with a few exceptions. The following observations can be made:

- Like results obtained by others [7, 8, 11] CO emissions generally increase at lower [O_2].
- At low [O_2] CO emissions are believed to be dominated by under-mixed fuel, as was noted in the introduction. Hence, despite the anticipated reduction in pre-ignition mixing due to the shortened ignition delay, increasing boost is beneficial to CO emissions due to (a) increased mixing rates throughout the cycle (Figure 13) and (b) decreased global equivalence ratio (Figure 7).
- At higher [O_2], larger CO emissions are observed at low load, despite a considerably lower equivalence ratio and less stringent mixing requirements. This behavior suggests that slow kinetic rates of CO oxidation associated with lean mixtures and lower average cylinder temperatures at low load are of greater importance. Recall that with increased boost ignition delay is reduced, and the formation of lean, slow-to-burn mixture becomes less likely. Moreover, as shown in Figure 18, burning rates of lean mixtures are greatly enhanced by increased pressure.
- Unlike UHC emissions from rich regions, homogeneous reactor simulations indicate that CO can result from bulk gas regions even when ϕ is slightly less than 1.

Regardless of the source of CO, Figure 20 demonstrates that increased boost is beneficial for CO emissions at all [O_2] and loads.

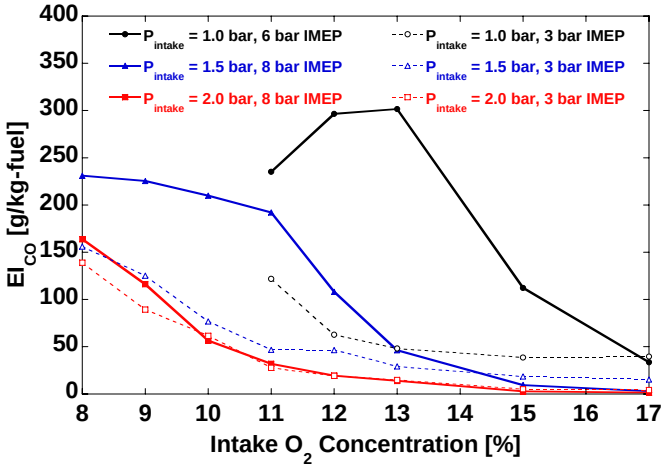

Figure 20. CO emissions indices for the O_2 concentration sweeps.

Perhaps the most unexpected CO behavior occurs at the 1.0 bar intake pressure, 6 bar IMEP condition, where CO emissions first increase rapidly with reduced O_2 concentration, and then start to decrease again upon further decreasing O_2 concentration. Similar behavior occurs to a lesser degree at the 1.5 bar boost, 8 bar IMEP condition, where CO emissions level off at lower [O_2]. This behavior occurs under conditions identified to have a strong potential for UHC storage in both squish volume quench layers and liquid films (Figures 16 and 19). Because the global equivalence ratio is rich for these operating conditions, energy release is primarily limited by O_2 availability, and fuel stored in this manner would reduce CO emissions while not strongly influencing heat release. Stored fuel can thus account for both the CO emissions behavior and the seemingly contradictory observation of approximately constant IMEP as [O_2] is reduced from 12% to 11% at 1.0 bar boost and 6 bar IMEP (Figure 4).

The reduced CO emissions and stable IMEP observed under these conditions may also be promoted by a second process. The early injection timing employed that promotes fuel storage in quench layers and liquid films can also promote formation of a more uniform bulk gas mixture, leading to more complete combustion of the available fuel. Kook et al. [8] showed numerically that for early injection, wherein a significant portion of the fuel is injected into the squish volume, the reentry of the fuel vapor into the bowl with the squish flow as the piston approaches TDC results in a broad, uniform spatial distribution of fuel in the bowl. This enhanced pre-mixing may assist in achieving a more complete combustion of the available fuel. The absence of a leveling off or decrease in CO emissions at the highest EGR levels in the results of Noehre et al. [7] is not inconsistent with this process. In their study, the wide, open-chamber piston used had little potential for film formation and no appreciable squish volume to assist with pre-mixing.

Combustion Efficiency and ISFC

The trends in UHC and CO emissions are closely mirrored in the combustion efficiency, shown in Figure 21. Combustion efficiencies are calculated from

$$\eta_c = 1 - \left(\frac{\dot{m}_{exhaust}}{\dot{m}_{Fuel}} \right) \frac{\sum_i y_i \Delta H_{R_i}}{\Delta H_{R,Fuel}} \qquad (1)$$

where y_i are the individual mass fractions and ΔH_{R_i} are the lower heating values of CO, H_2, and UHC (assumed to have the fuel composition) in the exhaust. Overall, combustion efficiency drops as O_2 concentration is lowered. Increased boost raises combustion efficiency, especially at lower [O_2] and higher loads, where combustion efficiency is worst. Better combustion efficiency is directly related to the reduction in UHC and CO emissions with increased boost pressure. At 2.0 bar boost, there seems to be little effect of load on combustion efficiency—decreased UHC at high load

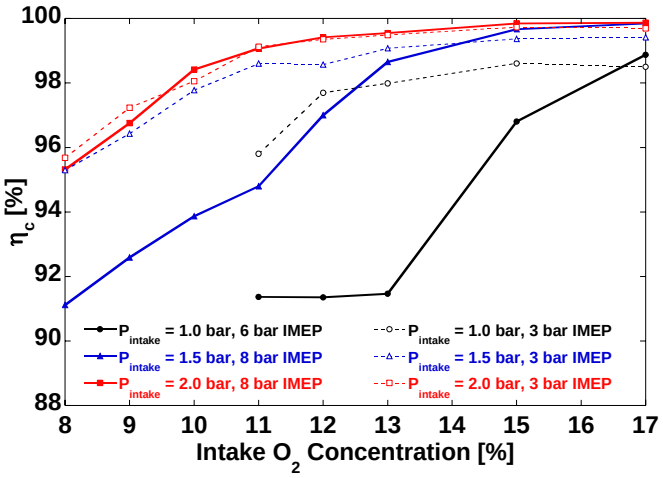

Figure 21. Combustion efficiencies for the O_2 concentration sweeps.

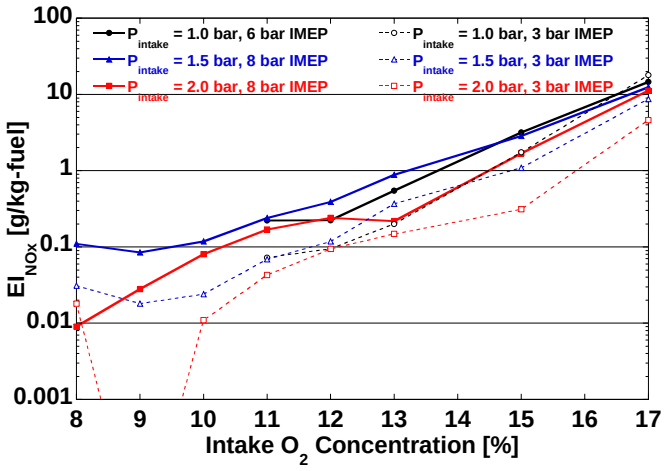

Figure 22. NO_x emissions indices for the O_2 concentration sweeps.

tends to be counterbalanced by generally increased CO. However, at lower boost pressures, higher combustion efficiencies were observed at the lower load condition, the only exceptions occurring at the highest O_2 concentrations.

The crossover in combustion efficiencies between load conditions as [O_2] varies suggests a change in combustion rate-limiting factors. Higher loads are expected to produce higher cylinder-average combustion temperatures, yielding increased reaction rates and shorter chemical time scales than lower load conditions provide. Therefore, for high load conditions exhibiting lower combustion efficiencies (occurring at low [O_2]) than low load conditions, mixing processes are expected to be the factor limiting combustion efficiency rather than chemical kinetics. On the other hand, at conditions where lower loads have lower combustion efficiencies (high [O_2]), chemical kinetics are suspected to be the combustion rate limiting factor for the low load conditions.

At the 1.0 bar boost, combustion efficiency at the 6 bar load levels off between 11% and 13% [O_2]. The fairly constant combustion efficiency follows from the trade-off between rising UHC emissions and falling CO emissions at that condition.

Trends in indicated specific fuel consumption (ISFC - not shown), similar to combustion efficiency, track emissions of UHC and CO well. Overall, ISFC improves with increasing [O_2]. The effect of increasing boost is to reduce ISFC, with the most significant improvements coming at low [O_2] and high load.

NO_x Emissions

Since one of the primary reasons for exploring LTC regimes is to reduce NO_x emissions, it is expected that as O_2 concentrations are decreased, NO_x emissions are reduced—as seen in Figure 22 on a semi-log scale. The naturally-aspirated boost condition produces similar NO_x levels to the 1.5 bar boost condition. However, the effect of increasing boost from 1.5 to 2.0 bar is to consistently reduce NO_x emissions for the entire range of O_2 concentrations tested at both high and low loads. NO_x formation rates are known to increase with both temperature and absolute O_2 concentration (i.e. partial pressure) [19]. Hence, with peak combustion temperatures approximately equal, we might expect the higher boost cases to produce more NO_x. For a given O_2 concentration, however, global equivalence ratios are reduced as boost increases (Figure 7). Mixing with cooler excess air available with higher boost levels likely suppresses the relatively slow NO_x formation process, leading to lower NO_x emissions. At higher load, mixing with excess air is reduced, and NO_x formation and emissions are higher, despite similar peak combustion temperatures.

A comparison to the evolution of NO_x with [O_2] in the heavy-duty engine studied by Noehre et al. [7] is presented in Figure 23 and shows excellent agreement, indicating that engine specific characteristics have very little influence on NO_x emissions. The heavy-duty engine data do not, however, show evidence of a consistent decrease in NO_x emissions with increasing boost as observed in our engine.

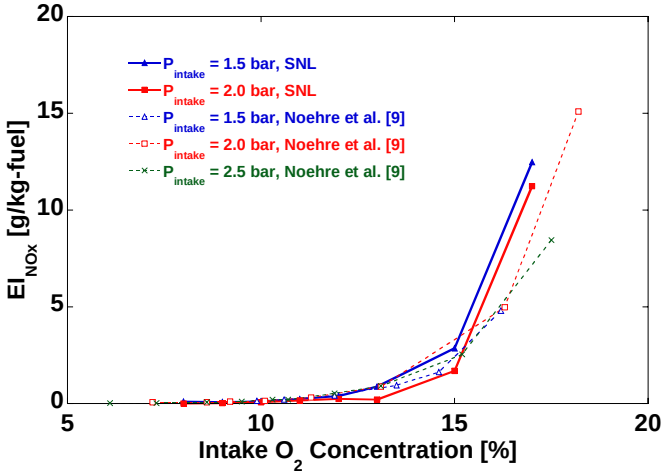

Figure 23. Comparison of NO_x emissions at 8 bar IMEP with the heavy-duty diesel study of Noehre et al. [9].

Soot Emissions

Soot emissions are shown in Figure 24. Soot levels are extremely low at the lower load condition, exhibiting no clear trend with [O_2]. The exception is for the highest boost condition at low load, where a typical soot "bump" is evident, albeit reduced by over a factor of 10 from the magnitude of the bump observed at higher load.

At the higher load, the peak of the soot bump moves toward lower [O_2] with increased boost. Idicheria and Pickett [29] demonstrated that, in free jets, the soot bump occurs due to the competition between falling soot formation rates at low combustion temperatures and increased time available for accumulation of soot as O_2 concentration is reduced. Furthermore, their modeling of soot formation in fuel jets [5] exhibited the same shift in the location of the peak toward lower [O_2] with increased ambient density as seen in Figure 24. However, Pickett and Idicheria find that the peak mass of soot formed increases with increased boost, while Figure 24 shows a 2-fold decrease in peak engine-out soot emissions as boost is increased. This reduction is thus likely due to enhanced soot oxidation at higher boost. The significant decrease in the B70–B90 burn times at high boost levels seen in Figure 13 is indicative of faster mixing rates during the latter part of the combustion event, when significant soot oxidation can be expected to be occurring. Enhanced oxidation can also change the shape of the soot bump and hence the location of the peak[5].

Noehre et al. [7] observed similar trends in the behavior of the soot bump as ambient density is increased. Their measurements, re-plotted against [O_2] were presented in Figure 1. Contrasting Figures 1 and 24, it is clear that while qualitative trends in the location of the soot bump are the same between the two studies, the changes are much more pronounced in the present study. We hypothesize that the influence of late-cycle oxidation is not as pronounced in their heavy-duty engine, and the peak engine-out soot emissions therefore do not change with boost. There is also a smaller shift in the peak toward low [O_2]—behavior which is also consistent with a lesser influence of oxidation processes.

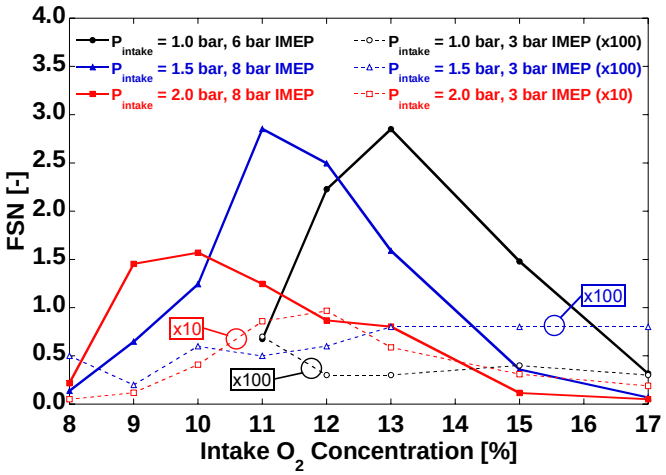

Figure 24. Soot filter smoke number levels for the O_2 concentration sweeps. Filter smoke numbers reported have not been corrected for skip-firing.

LATE-INJECTION LTC COMBUSTION

Cylinder Pressure Analysis

Figure 25 shows the MPRR observed in the SOI sweeps, which steadily declines at moderate load as SOI is retarded. At low load, the MPRR is reduced for both early and late SOI. The decrease in MPRR at late SOI is seemingly incompatible with the increasing ignition delay discussed below. Under these circumstances, falling temperature leading to slower reaction during the premixed combustion period is the probable source of the reduced noise. Like the behavior seen in the dilution-controlled combustion regime, increased boost generally reduces engine noise at the moderate load. At low load, and retarded SOI (where engine noise is not as significant), slight increases in MPRR were noted with increased boost. The increased MPRR is likely due to both higher temperatures during premixed combustion due to reduced ignition delay, coupled with more rapid reaction rates associated with the higher density.

Ignition delay times for the SOI sweeps are shown in Figure 26, along with ignition dwell. The evolution of these two parameters is identical, as they differ only by the fixed (for each load and boost level) injection duration. Differences in the injection duration cause the distinct separation in ignition dwell times between the high and low load cases, while for ignition delay there is little difference between load conditions. Ignition delay is shortest near SOI_c = -10°CA, increasing with both earlier and later injections. Shorter ignition delays correspond closely to injection timings providing higher bulk ambient temperatures during the ignition delay period. Like the dilution-controlled results shown in Figure 11, increasing boost causes a reduction in ignition delay, resulting in less premixing time before start of combustion. Again, the reduction in ignition delay occurs due to the higher absolute O_2 concentration (number density) at higher boost. Ignition dwell is negative only at higher load, and

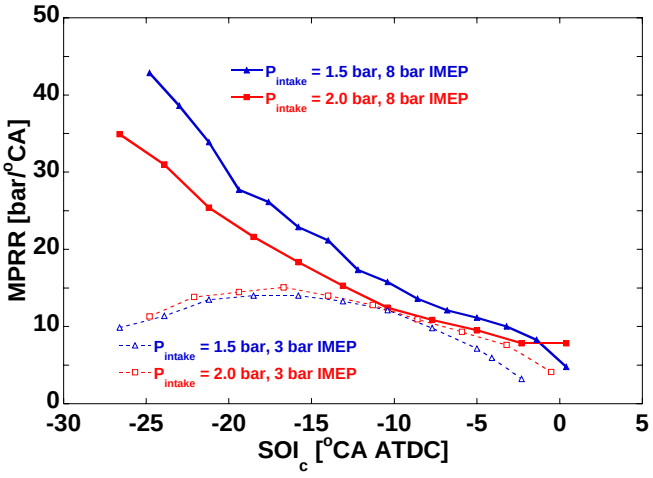

Figure 25. Maximum in-cylinder pressure rise rate for the SOI sweeps.

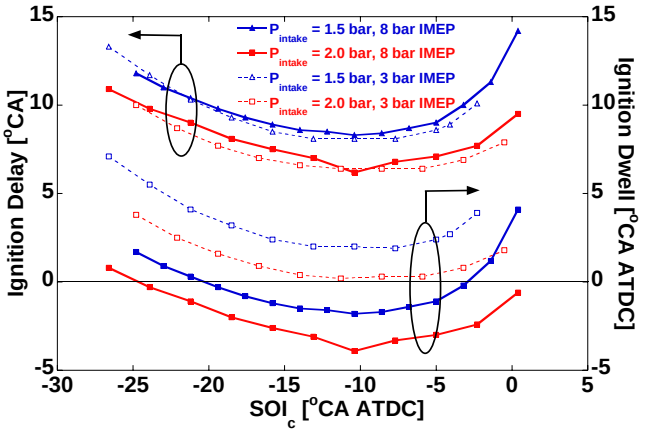

Figure 26. Ignition delay and ignition dwell for the SOI sweeps.

becomes more negative with increasing boost, signifying that more fuel is injected following the start of combustion.

Burn times from BA70 to BA90 are shown in Figure 27. Similar to the results of Figure 13, increased boost tends to reduce the duration of late-cycle, mixing-controlled combustion. There is also a trend toward shorter BA70–BA90 durations as SOI is retarded, which is more pronounced at low load.

UHC Emissions

UHC emissions increase as SOI is retarded, particularly at low load, as shown in Figure 28. Through examination of the instantaneous UHC signal [10], it has been shown that increased UHC at retarded SOI is partially attributable to increased bulk gas quenching—that is, combustion reactions in the bulk gases away from walls are quenched due to falling cylinder temperatures during expansion. UHC emissions are much higher at low loads, where the contribution to UHC from bulk gas quenching is expected to be especially prominent due to lower average cylinder temperatures.

Figure 29 shows fast-FID traces for two low-load cases

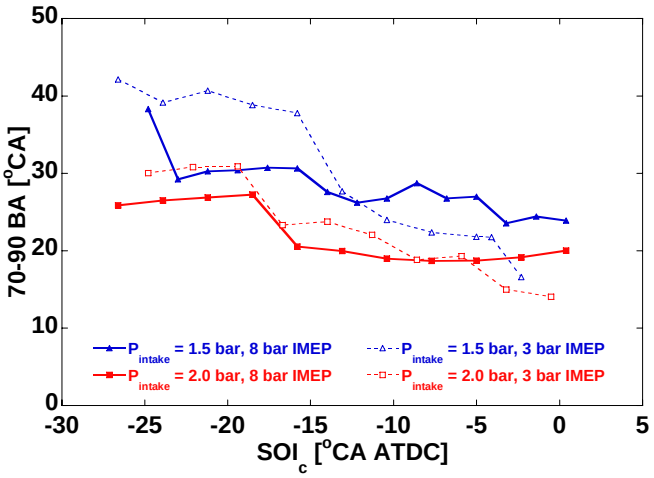

Figure 27. 70-90 burn angle times for the SOI sweeps, indicating the relative duration of the later mixing-controlled combustion.

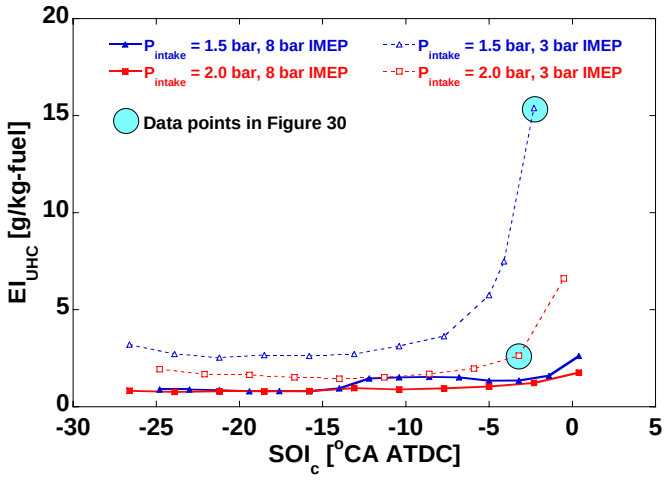

Figure 28. UHC emissions indices for the SOI sweeps. The filled circles designate data points which are examined more closely in Figure 29.

with similar late injection timings. Also indicated on Figure 29 is the period during the exhaust process when the bulk gas dominates the measured UHC. The lower level of UHC in the bulk gas and the smaller increase in UHC level during the bulk gas dominated period are strong evidence that less bulk gas quenching of combustion—leading to UHC emission—occurs at elevated boost. Increased mixing rates, evidenced by Figure 27, may help promote oxidation of late-to-mix rich regions. However, as proposed by Musculus et al. [20], over-lean mixtures formed by the last fuel injected could be a significant source of UHC for these low-load conditions. Additional evidence for the formation of over-lean regions is found in the CO emission behavior discussed below. Decreased ignition delay (Figure 26) and more rapid chemical reaction (Figure 18) associated with elevated boost will help reduce emissions from this source as well.

At the lower boost level, Figure 29 further shows that bulk gas UHC concentrations are higher in the latter portion of the exhaust stroke, corresponding to bulk

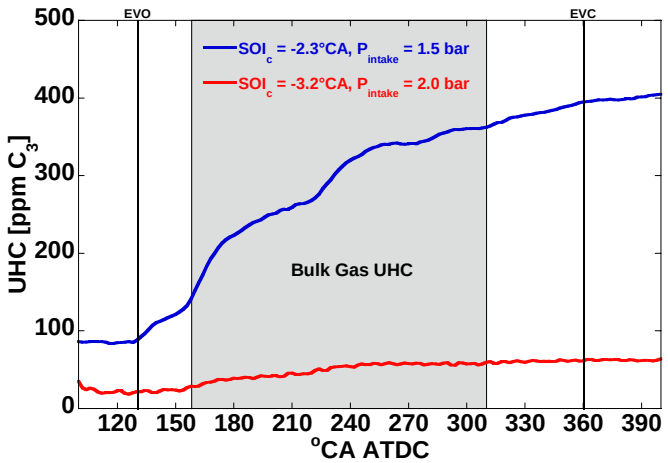

Figure 29. Fast-FID traces of cycle-resolved UHC emissions in the exhaust port. EVO and EVC times are indicated, as well as the period when bulk gas contributions to the UHC signal UHC dominate.

gases located lower in the cylinder at EVO. In contrast to the dilution-controlled combustion regime, there is no evidence that this behavior can be attributed to the delayed vaporization of liquid films. Liquid lengths calculated for the SOI sweeps are shown in Figure 30, where the potential liquid film formation region, as determined by the minimum piston impingement distance, is also indicated. The possibility of any liquid film formation exists only at very early injection timings, when measured UHC emissions are low.

Finally, the fast-FID traces (not shown) do not show evidence of significant squish volume quench layer UHC contributions, even for early SOI at this relatively moderate [O_2].

CO Emissions

Emissions of CO are shown in Figure 31. It is thought that, for conventional diesel combustion at light loads, CO emissions predominantly stem from over-lean fuel-air mixtures formed during the ignition delay period [14]. The strong correlation of CO emissions with ignition delay (Figure 26) suggests that this mechanism remains dominant at low loads for this moderate O_2 concentration.

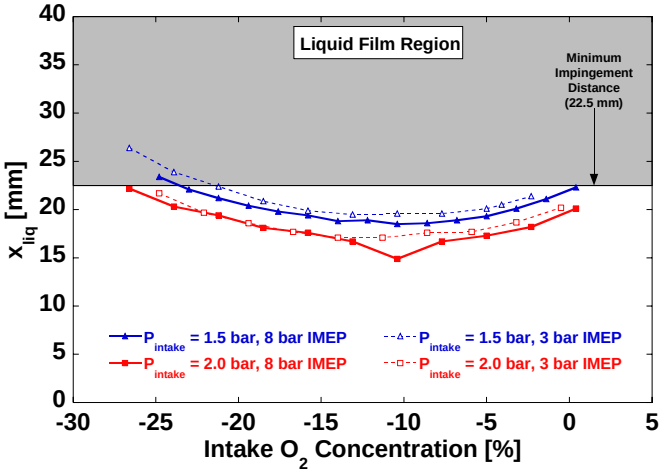

Figure 30. Estimated liquid lengths at 5.0° $ASOI_a$. The shaded region indicates a distance which is greater than the minimum required for liquid impingement.

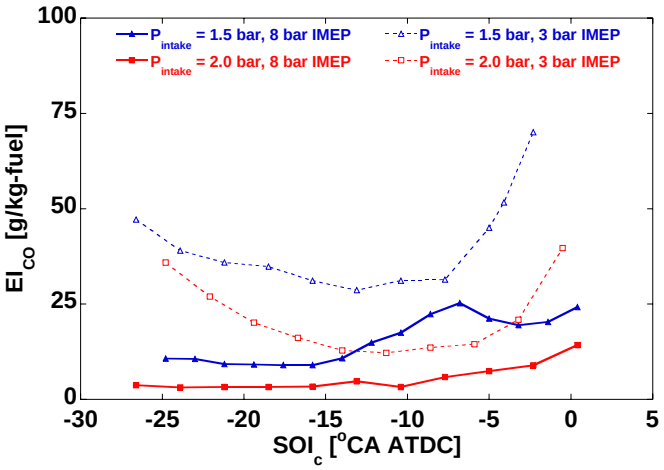

Figure 31. CO emissions indices for the SOI sweeps.

This suggestion is further supported by the sharp rise in CO emissions at retarded SOI, where the effects of increased ignition delay and increased ambient density on mixing are combined, leading to a high probability of forming excessively lean mixtures. Increased boost is expected to reduce formation of over-lean regions (and hence CO emissions), since the strongly reduced ignition delay will dominate over increased mixing rates. Increased reaction rates promoted by increased boost (Figure 18) undoubtedly also assist in promoting rapid CO oxidation.

At the higher loads, CO emissions are considerably reduced. Like the UHC emissions described above, this behavior is consistent with reduced quenching of oxidation reactions due to higher average cylinder temperatures. Lower CO emissions at higher load provide additional evidence that the contribution to CO emissions of over-lean mixtures dominates over the contribution from over-rich mixtures at light load.

CO and UHC emissions generally track each other closely. Nevertheless, at low load and advanced SOI, CO emissions increase considerably, while UHC emissions change little. Combustion of both lean and moderately rich mixtures could produce this behavior. Rich mixtures with ϕ less than approximately 2 can produce CO without significant UHC (Figure 17). It is unlikely, however, that advancing SOI results in richer mixtures—lean mixtures are much more likely to be produced. For lean mixtures, the oxidation of CO can take considerably longer than the destruction of hydrocarbons, a phenomenon that is illustrated in Figure 32 at a pressure representative of our 1.5 bar intake pressure condition. We believe this delayed oxidation of CO is the cause of the increasing light-load CO emissions observed at early SOI.

Finally, in line with conventional diesel behavior at moderate to high loads, the local peak in CO emissions observed at high-load and 1.5 bar boost mirrors the soot behavior discussed below. Because soot only forms in the products of rich combustion, this indicates that at this

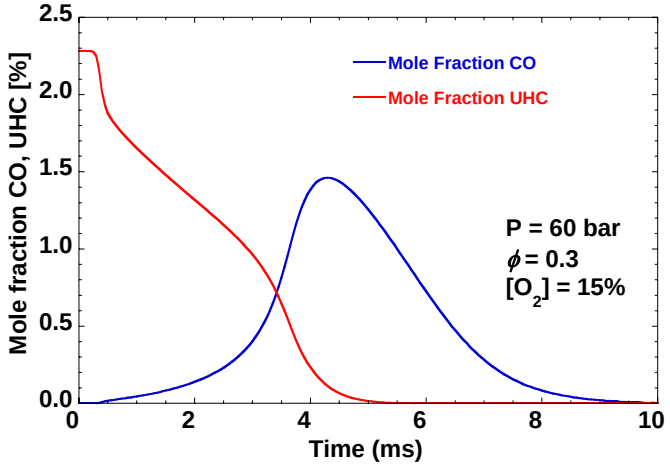

Figure 32. Constant volume oxidation history of UHC and CO of a ϕ = 0.3 mixture in a 60 bar, 15% [O_2] atmosphere.

boost level, the high load CO emissions have a significant component associated with rich fuel regions that fail to mix with sufficient oxygen before falling cylinder temperatures quench CO oxidation. A similar, though smaller, feature can be seen in the high load UHC behavior of Figure 28.

Combustion Efficiency and ISFC

As shown in Figure 33, combustion efficiency (calculated with Equation 1) is consistent with the UHC and CO emissions shown in Figures 28 and 31. Decreases in combustion efficiency correlate with increased (or flat) UHC and increased CO emissions. Combustion efficiency is highest at intermediate SOI and high load. The effect of increased boost pressure is to raise combustion efficiency at both load conditions. Increases in combustion efficiency are especially large at low load and the most retarded injection timings—where the biggest reduction in UHC and CO emissions was also observed. Furthermore, fuel consumption also benefits from increased boost, with an increasing improvement in ISFC (not shown) coming as SOI is retarded.

NO_x Emissions

Changes in boost pressure have little effect on NO_x emissions in the late-injection LTC regime at low load (Figure 34). At moderate load, however, increased boost yields slightly higher NO_x emissions for near-TDC SOI. This is likely caused by a reduced ignition delay at high boost, which leads to higher in-cylinder temperatures during combustion. For early SOI, increasing boost pressure tends to lower NO_x emissions at both load conditions, similar to the behavior observed in the dilution-controlled combustion regime discussed above. Low loads produce less engine-out NO_x than high load, no doubt due in part to lower peak flame temperatures as well as post-combustion mixing with cooler excess air.

Soot Emissions

Figure 35 shows that a "bump" in soot emissions is observed when injection is retarded at constant $[O_2]$,

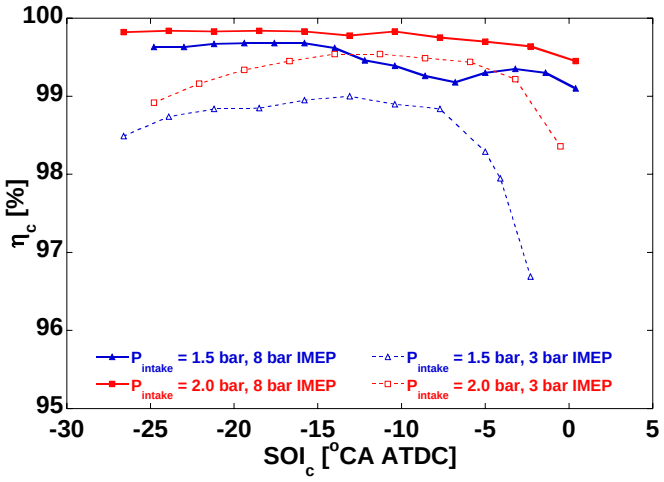

Figure 33. Combustion efficiencies for the SOI sweeps.

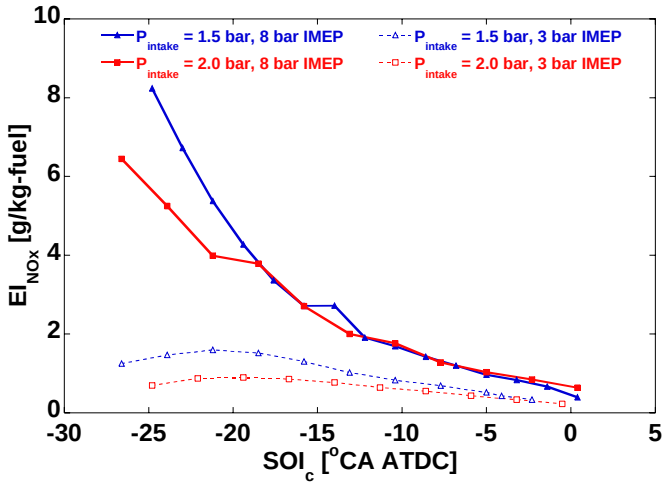

Figure 34. NO_x emissions indices for the SOI sweeps.

much like the soot emission behavior observed with varying $[O_2]$. While detailed in-cylinder measurements will be required to identify the precise cause of the bump, we hypothesize that its existence is due to a trade-off involving the following factors:

1) As injection is initially retarded, ignition delay decreases to a minimum near SOI$_c$ = -10°CA (Figure 26). In the absence of significant changes in early mixing behavior, the average mixture composition at ignition is becoming richer during this period—promoting greater formation of soot. Retarding SOI further, ignition delay increases and produces leaner mixtures and less soot formation.

2) For all SOI, retarding injection serves to decrease the average cylinder pressure during the period when significant soot formation occurs. Likewise, for the same initial equivalence ratio, the temperature of the sort forming products of the premixed burn will be decreasing. Both of these factors should serve to decrease soot formation.

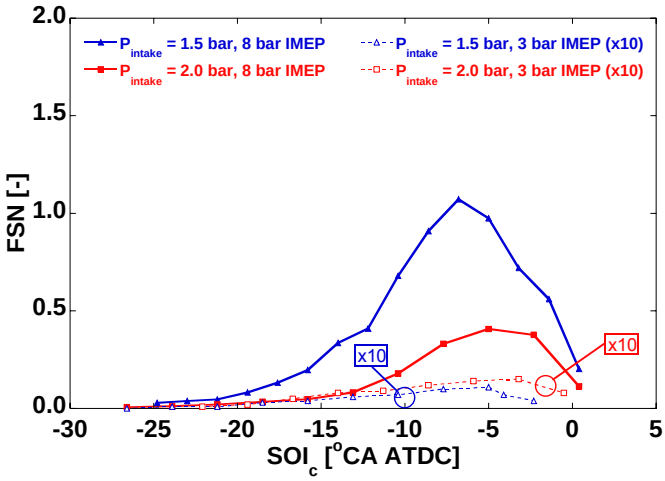

Figure 35. Soot filter smoke numbers for the SOI sweeps. Note this data reflects skip-fired conditions wherein the engine was fired only once every 4 cycles. Filter smoke numbers reported have not been corrected for skip-firing.

3) Retarded SOI leaves less time for soot oxidation, and falling pressure and temperature will reduce soot oxidation rates. These lower expected oxidation rates, coupled with the rapidly decreasing soot emissions, unequivocally point to a sharp reduction in formation at the latest injection timings.

At high load, increasing boost clearly reduces soot emissions. As discussed previously, we expect the decreased ignition delay associated with highly boosted conditions to dominate over improved pre-ignition mixing. Hence, richer mixtures are expected at ignition. Likewise, higher pressures will promote soot formation. The reduction in soot emissions must thus be associated with improved oxidation rates, due to higher post-soot-formation mixing rates. These higher mixing rates are apparent in the reduced B70-B90 burn times shown in Figure 27.

At low load, increased boost slightly increases measured soot emissions. However, soot emissions are extremely low. It is possible that at these lower average (global) equivalence ratios, the enhanced mixing associated with higher boost is less important, and cannot overcome the disadvantages of richer mixtures at ignition and increased formation due to high pressure.

Overall, the combustion performance and emissions presented in this section indicate that by increasing boost pressure, it is possible to significantly improve the performance of late-injection LTC strategies, simultaneously achieving reductions in UHC, CO , NO_x, and soot emissions, while improving combustion efficiency and pressure rise (noise) characteristics. By reducing CO, UHC and soot (at high load), while not affecting NO_x, increased boost allows a larger window of injection timing in which all emissions are acceptable, thus facilitating engine control. Finally, the considerable reductions in engine-out soot at higher loads with increased boost pressure shows that late-injection LTC operation can be extended to higher loads with some degree of turbocharging.

COMPARATIVE EVALUATION OF LTC STRATEGIES

To evaluate the relative performance of the two LTC strategies, this section compares the emissions and efficiency observed at both load conditions for a fixed NO_x emission level of 0.5 g/kg-fuel. Comparisons of noise, emissions levels, and combustion efficiencies have been made at both the 1.5 bar and 2.0 bar intake pressures.

A comparison of engine noise is shown in Figure 36 in terms of maximum pressure rise rates. Late-injection LTC reduces engine noise at each condition, and by as much as 64% at an intake pressure of 1.5 bar and moderate load. Reductions of MPRR at other conditions ranged from 5% to 48%.

Emissions other than NO_x, which has been fixed at 0.5 g/kg-fuel (0.64 g/kg-fuel at 2.0 bar boost moderate load),

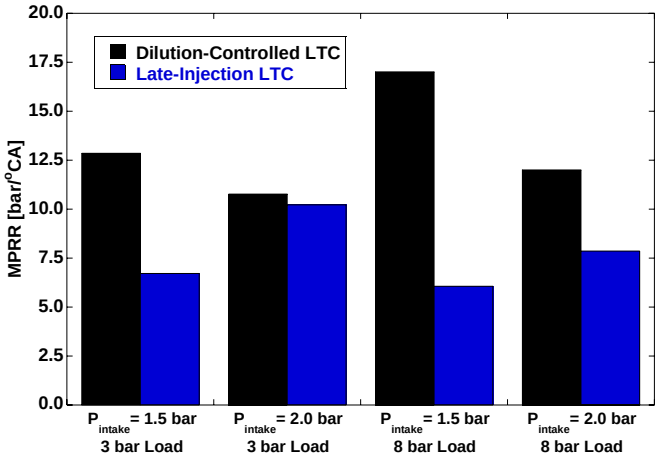

Figure 36. Comparison of maximum pressure rise rate (engine noise) between the dilution-controlled and late-injection LTC regimes at a fixed NO_x emissions index of 0.5 g/kg-fuel.

are shown in Figures 37 through 39. Late-injection LTC yields an increase in UHC emissions compared to dilution-controlled LTC, especially at the lower intake pressure, low-load condition—where a 245% increase in UHC emissions was observed (increases ranged from 30% to 110% at other conditions). The absolute levels of UHC emissions levels are consistent with US Tier II, Bin 5 emissions levels if the vehicle is equipped with a moderate efficiency oxidation catalyst, with the possible exception of the late-injection low-load, low-boost case.

Concerning CO emissions, late-injection LTC generally has higher CO emissions than dilution-controlled LTC, with the major exception being the 1.5 bar intake pressure, moderate load condition (Figure 38). At that condition, CO emissions are rising rapidly as $[O_2]$ decreases, hence the elevated CO levels. All absolute CO levels are consistent with legislated emissions levels assuming a modest efficiency for the catalyst.

Our results show that soot is generally lower for late-injection LTC than for dilution-controlled LTC (Figure 39). At low load, soot is extremely low for both LTC

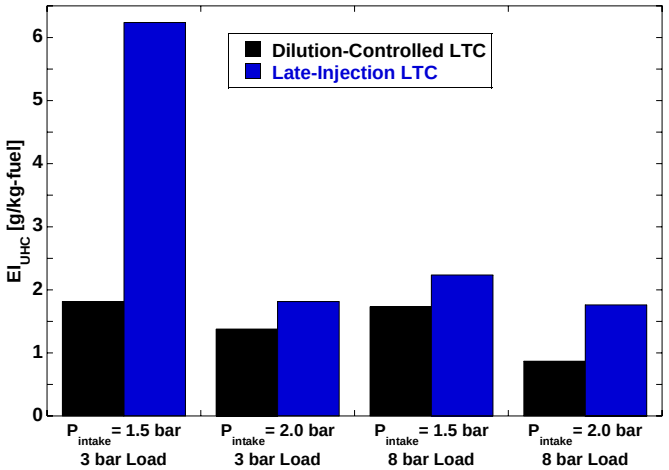

Figure 37. UHC emissions comparison between the dilution-controlled and late-injection LTC regimes at a fixed NO_x emissions index of 0.5 g/kg-fuel.

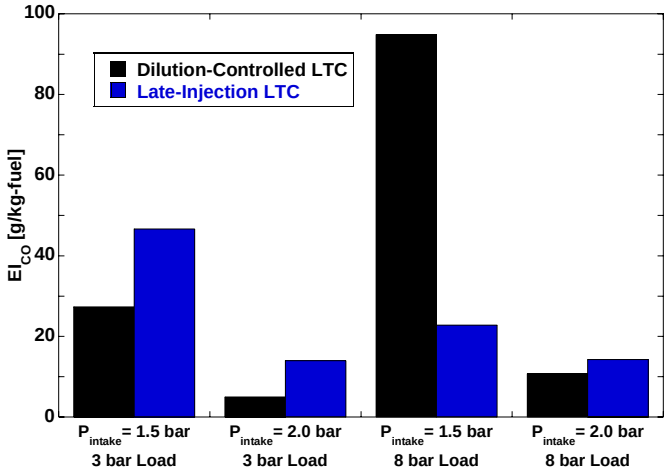

Figure 38. CO emissions comparison between the dilution-controlled and late-injection LTC regimes at a fixed NO_x emissions index of 0.5 g/kg-fuel.

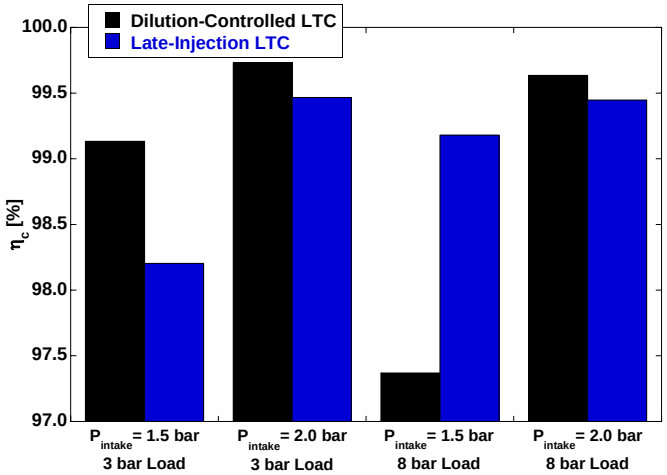

Figure 40. Combustion efficiency comparison between the dilution-controlled and late-injection LTC regimes at a fixed NO_x emissions index of 0.5 g/kg-fuel.

strategies. However, at moderate load—where soot levels are significant—late-injection LTC offers a reduction in soot of between 75% and 85% below dilution-controlled LTC levels.

Combustion efficiencies are between 0.25% and 0.9% higher for dilution-controlled LTC than for late-injection LTC, as shown in Figure 40. The exception occurs at the 1.5 bar boost, moderate load condition, where combustion efficiency is dropping off with decreasing $[O_2]$ due to rapid increases in CO emissions for the dilution-controlled LTC regime. Note that, in general, combustion efficiencies are quite good. Combustion efficiencies at all but two operating conditions exceed 99%.

Finally, a comparison of indicated specific fuel consumption (ISFC) between the two LTC strategies is shown in Figure 41. The comparison is made in terms of the percent improvement (reduction) in ISFC for the dilution-controlled conditions versus the late-injection conditions. Across the range of operating conditions, dilution-controlled LTC has better ISFC, ranging from an improvement of between 1.6% and 9.9%. Better ISFC, even under conditions of lower combustion efficiency (P_{int} = 1.5 bar, 8 bar IMEP), is likely due to the more advantageous combustion phasing associated with the dilution-controlled strategy, but coupled with a poor work conversion efficiency at that condition.

SUMMARY AND CONCLUSIONS

A systematic study characterizing the effect of increased boost pressure on engine performance and emissions for two LTC regimes in a small-bore, light-duty diesel engine are presented. Cylinder pressure derived performance metrics, UHC, CO, NO_x, and soot emissions, as well as combustion efficiency are provided for a range of intake pressures spanning 1.0 to 2.0 bar boost. At each condition both low and moderate loads were investigated.

Increased boost pressure shows promise for limiting UHC and CO emissions in both LTC combustion

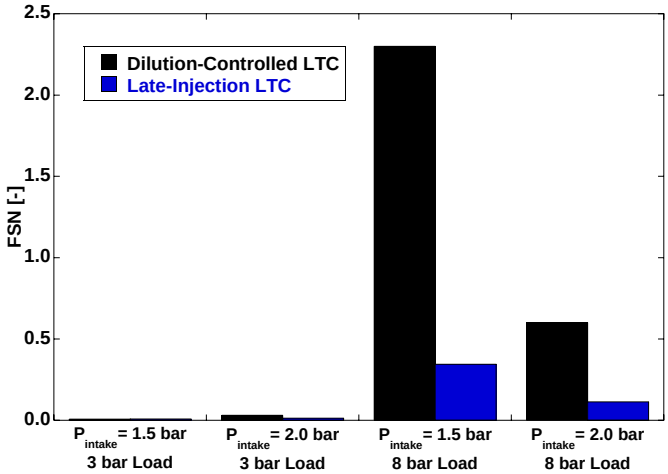

Figure 39. Soot comparison between the dilution-controlled and late-injection LTC regimes at a fixed NO_x emissions index of 0.5 g/kg-fuel. Filter smoke numbers reported have not been corrected for skip-firing.

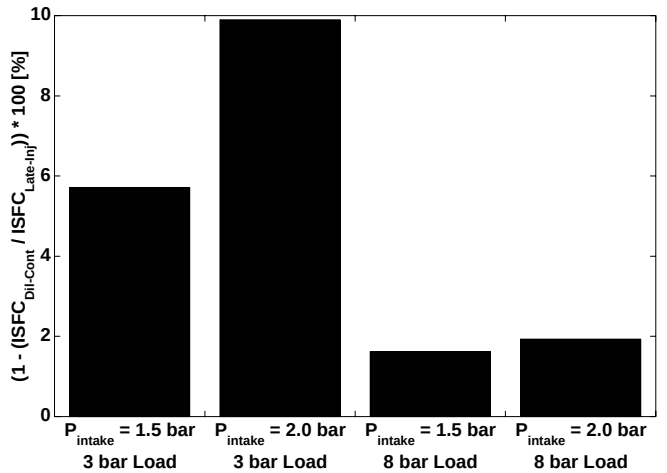

Figure 41 Comparison of indicated specific fuel consumption (ISFC) between the dilution-controlled and late-injection LTC regimes at a fixed NO_x emissions index of 0.5 g/kg-fuel.

regimes. Further benefits of increased boost pressure include reduced NO_x emissions, reduced peak soot levels, and increased combustion efficiency. At low oxygen concentrations, however, increased boost can negatively impact soot emissions. The results show that turbocharging is beneficial not only from an efficiency and power density standpoint, but also in terms of engine-out emissions. Furthermore, higher intake pressures result in lower cylinder pressure rise rates and a reduction in engine noise at higher loads, where engine noise is loudest.

Overall, dilution-controlled LTC yields lower UHC and CO emissions with better combustion efficiency and ISFC than late-injection LTC. The exception occurs at the 1.5 bar boost moderate load condition, where CO is rapidly rising as $[O_2]$ decreases, yielding much higher CO emissions and consequently lower combustion efficiency for dilution-controlled LTC than for late-injection LTC. On the other hand, late-injection LTC shows improvements in engine noise and soot over dilution-controlled LTC.

ACKNOWLEDGMENTS

Support for this research was provided by the United States Department of Energy, Office of FreedomCAR and Vehicle Technologies. The research was performed at the Combustion Research Facility, Sandia National Laboratories, Livermore, California. Sandia is a multiprogram laboratory operated by Sandia Corporation, a Lockheed Martin Company, for the United States Department of Energy's National Nuclear Security Administration under contract DE-AC04-94AL85000. The authors are grateful to General Motors for providing the engine head, as well as for their input into the project. The authors also thank Kenneth St. Hilaire, Lloyd Claytor, Dave Cicone, and Gary Hubbard of Sandia National Laboratories for their assistance in the laboratory, and to Manuel Gonzalez of the University of Wisconsin for his timely technical assistance.

REFERENCES

1. Naber, J. D. and Siebers, D. L., "Effects of Gas Density and Vaporization on Penetration and Dispersion of Diesel Sprays," SAE paper 960034, *SAE Transactions*, v. 105, 1996.
2. Siebers, D. L., "Liquid-Phase Fuel Penetration in Diesel Sprays," SAE paper 980809, *SAE Transactions*, v. 107, 1998.
3. Siebers, D. L. and Higgins, B., "Flame Lift-Off on Direct-Injection Diesel Sprays Under Quiescent Conditions," SAE paper 2001-01-0530, *SAE Transactions*, v. 110, 2001.
4. Pickett, L. M., Siebers, D. L. and Idicheria, C. A., "Relationship Between Ignition Processes and the Lift-Off Length of Diesel Fuel Jets," SAE paper 2005-01-3843, *SAE Transactions*, v. 114, 2005.
5. Pickett, L. M. and Idicheria, C. A., "Effects of Ambient Temperature and Density on Soot Formation under High-EGR Conditions," Proc. of THIESEL Conference on Thermo- and Fluid Dynamic Processes in Diesel Engines, Sep. 13-15, Valencia, Spain, 2006
6. Tanin, K. V., Wickman, D. D., Montgomery, D. T., Das, S. and Reitz, R. D., "The Influence of Boost Pressure on Emissions and Fuel Consumption of a Heavy-Duty Single Cylinder D. I. Diesel Engine," SAE paper 1999-01-0840, *SAE Transactions*, v. 108, 1999.
7. Noehre, C., Andersson, M., Johansson, B. and Hultqvist, A. "Characterization of Partially Premixed Combustion," SAE paper 2006-01-3412, 2006.
8. Kook, S., Bae, C., Miles, P. C., Choi, D., Bergin, M. and Reitz, R. D. "The Effect of Swirl Ratio and Fuel Injection Parameters on CO Emission and Fuel Conversion Efficiency for High-Dilution, Low-Temperature Combustion in an Automotive Diesel Engine," SAE paper 2006-01-0197, 2006.
9. Opat, R., Ra, Y., Gonzalez D., M. A., Krieger, R., Reitz, R. D., Foster, D. E., Durrett, R. P. and Siewert, R. M. "Investigation of Mixing and Temperature Effects on HC/CO Emissions for Highly Dilute Low Temperature Combustion in a Light Duty Engine," SAE paper 2007-01-0193, 2007.
10. Colban, W. F., Miles, P. C. and Oh, S. "On the Cyclic Variability and Sources of Unburned Hydrocarbon Emissions in Low Temperature Diesel Combustion Systems," SAE paper 2007-01-1837, 2007.
11. Akihama, K., Takatori, Y., Inagaki, K., Sasaki, S. and Dean, A. M., "Mechanism of the Smokeless Rich Diesel Combustion by Reducing Temperature," SAE paper 2001-01-0655, *SAE Transactions*, v. 110, 2001.
12. Weiβäck, M., Csató, J., Glensvig, M., Sams, T. and Herzog, P., "Alternative Brennverfahren: Ein Ansatz für den zukünftigen Pkw-Dieselmotor," *Motortechnische Zeitschrift*, v. 64, pp. 718-727, 2003.
13. Kimura, S., Aoki, O., Ogawa, H., Muranaka, S. and Enomoto, Y., "New Combustion Concept for Ultra-Clean and High-Efficiency Small DI Diesel Engines," SAE paper 1999-01-3681, *SAE Transactions*, v. 108, 1999.
14. Kook, S., Bae, C., Miles, P. C., Choi, D. and Pickett, L. M., "The Influence of Charge Dilution and Injection Timing on Low-Temperature Diesel Combustion and Emissions," SAE paper 2005-01-3837, *SAE Transactions*, v. 114, 2005.
15. Private communication, 2006, Opat, R., Krieger, R., Gonzalez D., M. A., Foster, D. E. and Ra, Y., "Low Temperature Diesel Combustion Sources and Mechanisms of HC/CO Emissions."
16. Kee, R. J., Rupley, F. M., Miller, J. A., Coltrin, M. E., Grcar, J. F., Meeks, E., Moffat, H. K., Lutz, A. E., Dixon-Lewis, G., Smooke, M. D., Warnatz, J., Evans, G. H., Larson, R. S., Mitchell, R. E., Petzold, L. R., Reynolds, W. C., Caracotsios, M., Stewart, W. E., Glarborg, P., Wang, C., McLellan, C. L., Adigun, O., Houf, W. G., Chou, C. P., Miller, S. F., Ho, P., Young, P. D., Young, D. J., Hodgson, D. W., Petrova, M. V. and Puduppakkam, K. V., CHEMKIN Release 4.1, Reaction Design, Inc., San Diego, CA, 2006.
17. http://www-cmls.llnl.gov/?url=science_and_technology-chemistry-combustion-nc7h16
18. http://www.me.berkeley.edu/gri_mech/

19. Heywood, J. B., Internal Combustion Fundamentals, McGraw-Hill, Inc., New York, 1988.
20. Musculus, M. P. B., Lachaux, T., Pickett, L. M. and Idicheria, C. A. "End-of-Injection Over-Mixing and Unburned Hydrocarbon Emissions in Low-Temperature-Combustion Diesel Engines," SAE paper 2007-01-0907, 2007.
21. Greeves, G., Khan, I. M., Wang, C. H. T. and Fenne, I., "Origins of Hydrocarbon Emissions from Diesel Engines," SAE paper 770259, *SAE Transactions*, v. 86, 1977.
22. Siebers, D. L., "Scaling Liquid-Phase Fuel Penetration in Diesel Sprays Based on Mixing-Limited Vaporization," SAE paper 1999-01-0528, *SAE Transactions*, v. 108, 1999.
23. Curran, H. J., Fisher, E. M., Glaude, P.-A., Marinov, N. M., Pitz, W. J., Westbrook, C. K., Layton, D. W., Flynn, P. F., Durrett, R. P., zur Loye, A. O., Akinyemi, O. C. and Dryer, F. L., "Detailed Chemical Kinetic Modeling of Diesel Combustion with Oxygenated Fuels," SAE paper 2001-01-0653, *SAE Transactions*, v. 110, 2001.
24. Pickett, L. M. and Siebers, D. L., "Soot in Diesel Fuel Jets: Effects of Ambient Temperature, Ambient Density, and Injection Pressure," *Combustion and Flame*, v. 138, pp. 114-135, 2004.
25. Higgins, B. S., Mueller, C. J. and Siebers, D. L., "Measurements of Fuel Effects on Liquid-Phase Penetration in DI Sprays," SAE paper 1999-01-0519, *SAE Transactions*, v. 108, 1999.
26. Kashdan, J. T., Mendez, S. and Bruneaux, G. "On the Origin of Unburned Hydrocarbon Emissions in a Wall-Guided, Low NO_x Diesel Combustion System," SAE paper 2007-01-1836, 2007.
27. Stevens, E. and Steeper, R., "Piston Wetting in an Optical DISI Engine: Fuel Films, Pool Fires, and Soot Generation," SAE paper 2001-01-1203, *SAE Transactions*, v. 110, 2001.
28. Li, J., Matthews, R. D., Stanglmaier, R. H., Roberts, C. E. and Anderson, R. W., "Further Experiments on the Effects of In-Cylinder Wall Wetting on HC Emissions from Direct Injection Gasoline Engines," SAE paper 1999-01-3661, *SAE Transactions*, v. 108, 1999.
29. Idicheria, C. A. and Pickett, L. M., "Soot Formation in Diesel Combustion under High-EGR Conditions," SAE paper 2005-01-3834, *SAE Transactions*, v. 114, 2005.

NOMENCLATURE

$ASOI_a$	After the Actual Start of Injection
BA10	10% Burn Angle
BA70	70% Burn Angle
BA90	90% Burn Angle
BTDC	Before Top Dead Center
C_p	Specific Heat at Constant Pressure
C_v	Specific Heat at Constant Volume
CA	Crank Angle
CO	Carbon Monoxide
COV	Coefficient of Variation
CR	Compression Ratio
DCCS	Dilution-Controlled Combustion System
EGR	Exhaust Gas Recirculation
EI	Emissions Index
EOI	End of Injection
EVC	Exhaust Valve Closing
EVO	Exhaust Valve Opening
FID	Flame Ionization Detector
FSN	Filter Smoke Number
$H_{R,Fuel}$	Lower Heating Values of Fuel
H_{Ri}	Lower Heating Values of CO, H_2, and UHC
IMEP	Indicated Mean Effective Pressure
ISFC	Indicated Specific Fuel Consumption
IVC	Intake Valve Closing
IVO	Intake Valve Opening
LTC	Low Temperature Combustion
$\dot{m}_{exhaust}$	Mass Flow Rate of Exhaust
$\dot{m}_{fuel}$	Mass Flow Rate of Fuel
MBT	Maximum Brake Torque
MK	Modulated Kinetics
MPRR	Maximum Pressure Rise Rate
NO_x	Nitrogen Oxides
P_{ex}	Exhaust Pressure
P_{intake}	Intake (Boost) Pressure
PPCI	Partially Premixed Compression Ignition
R_s	Swirl Ratio
S	Spray Penetration Distance (Vapor)
SOI	Start of Injection
SOI_a	Actual Start of Injection
SOI_c	Start of injection Command
TDC	Top Dead Center
UHC	Unburned Hydrocarbons
x_{liq}	Fuel Jet Liquid Penetration Length
y_i	Individual Exhaust Mass Fractions
ϕ	Equivalence Ratio
ϕ_{avg}	Average In-Cylinder Equivalence Ratio
η_c	Combustion Efficiency
θ	Spray Dispersion Angle
ρ_{amb}	Ambient In-Cylinder Density